

THE RATE AND THE MECHANISM OF THE REACTIONS
OF HYDROGEN SULFIDE WITH THE BASIC MINERALS IN COAL

A. Attar and F. Dupuis

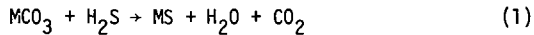
Department of Chemical Engineering
University of Houston

1.0 INTRODUCTION

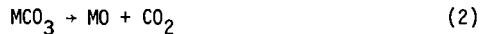
The inorganic matter in coal can be classified into three groups of minerals according to their reactions with hydrogen sulfide (H_2S): (1) basic minerals, (2) minerals with catalytic activity, and (3) inert minerals. In the range of temperatures 200-900°C, most of the minerals are inert or have a slight catalytic activity on the rate of decomposition of H_2S . However, the basic minerals react with H_2S and the corresponding sulfides are formed. The most important minerals in this category are calcite (trigonal $CaCO_3$), aragonite (orthorhombic $CaCO_3$), dolomite ($CaCO_3 \cdot MgCO_3$), sidrite ($FeCO_3$), and to some extent montmorillonite (clay) (Attar, 1977).

The systems of reaction between H_2S and a metal carbonate MCO_3 involves four reactions (Glund *et al.*,²(1930), Stinnes (1930), Bertrand (1937), Parks (1961), and Squires (1972)).

1. Direct reaction of the carbonate with H_2S :



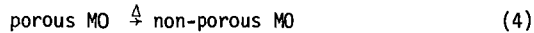
2. Decomposition of the carbonate to the oxide MO and CO_2 :



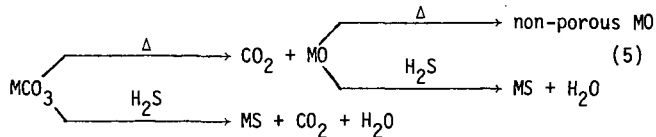
3. Reaction between the oxide and H_2S :



4. Sintering of the oxide and the formation of non-porous materials.



Reactions 1. and 2. are parallel, and reactions 3. and 4. are parallel. The last two reactions are in series with reaction 2.



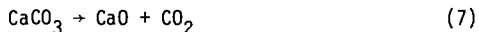
H_2S is formed in coal by the reactions of FeS_2 with hydrocarbons and H_2 , (Powell, 1921) and by the decomposition of the organic sulfur compounds Thiessen (1945). In particular, H_2S is formed when the sulfidic functional groups decompose to H_2S and an olefin. The H_2S can react with the basic minerals and thus, the sulfur is trapped in the char in the form of the sulfide (Armstrong 1939). The kinetics of the reactions of H_2S with calcined dolomite and calcite were studied by Squires and co-workers (1970, 1972). In the present work, the mechanism of the reaction, their rate, and rate constants were derived for the reactions of H_2S with calcite, sidrite, dolomite, and montmorillonite.

Complete conversion of dolomite to CaS and MgCO₃ is obtainable at 570°C, but only 1.8-2.9 Wt. % of -200 mesh calcite reaction at these conditions (2.1 m²/gm surface area). At 700°C calcite and dolomite react at essentially identical rates. The rate of reaction of dolomite is however very sensitive to impurities.

Different rate controlling steps limit the apparent rate of consumption of H₂S at different temperatures. The rate controlling step depends also on the particular material and on its crystalline structure. At low temperatures, the rate is controlled by the rate of mass transfer and by the rate of diffusion of CO₂ in MS. At intermediate temperatures, the rate of consumption of H₂S is controlled by the availability of free surface of MO or MCO₃. In this range of temperature, the carbonates decompose according to reaction 2, a new surface is thus exposed which is not covered by MS, thus, the effective rate of consumption of H₂S increases. The available surface decreases by sintering when the temperature is too high, thus the rate of consumption of H₂S may decrease. When the rate of decomposition of MCO₃ becomes very large, the rate of consumption of H₂S may be limited by mass transfer in the gas.

The crystalline structure of calcite and dolomite is trigonal (Bragg *et al.* (1965) p. 127) and is basically identical, except that in dolomite alternate Ca⁺² ions are replaced by Mg⁺² ions. The spacial dimensions are different because the ionic radius of Mg⁺² is 0.65 Å and that of Ca⁺² is 0.99 Å (Greenwood, 1970). The mechanism of their reaction is however very different.

The rate of reaction of pure dolomite with H₂S is almost constant, and, does not vary with the conversion (up to 30 Wt. % conversion). Impure dolomite reacts initially at a much larger rate then after some of it had been converted. At 570°C the rate drops to about half the initial rate after about 4% of the material had been converted. At 570°C calcite reacts initially at about the same rate as pure dolomite, however, the rate of reaction drops to nil very rapidly. We estimate that when a layer of about 7.8 molecules of CaS, on the average, is formed on the surface of calcite, the diffusion of H₂S is blocked and the reaction stops. The layer of CaS breaks at around 635-650°C when the "pressure" of CO₂ inside the CaCO₃ crystal due to the decomposition reaction



becomes excessive. When the CaS layer breaks, a new surface is exposed and the reaction can proceed. Around 700°C no difference could have been detected between the rate of reaction of calcite and dolomite.

2.0 EXPERIMENTAL

Figure 1 is a schematic flow diagram which shows the relations among the various parts of the system.

The experimental system consists of four major components: (1) a differential reactor, (2) a pulse injector, (3) a gas chromatograph with a TC detector, and (4) an integrator with a data system.

Figure 2 shows the differential reactor. The shell (1), the tube (2), and the fillers (3) are made out of quartz. The gas inlet and outlet are through a SS connector. The quartz reactor is inserted through the wall of a high temperature furnace which temperature is controlled and monitored.

Pulses of the reactive gas, H_2S , are fed using a microprocessor controlled gas-chromatograph injector. The size of the injector loop determines the size of the pulse of H_2S which is introduced into the stream of helium. The helium passed through the reactor and into a chromatographic column and detector.

Each pulse of H_2S which is injected into the reactor resulted in a pulse which consists of the reaction products plus the unreacted H_2S . The mixture of gases is separated on the column and detected by the TC detector. The signal from the detector is integrated by a microprocessor which multiplies the areas by the proper calibration factors and prints the amounts of each component in the pulse of products of the reaction. The integrator and the injector are synchronized so that periodic operation is possible.

The repeatability of the injections was 0.05% or better. The overall accuracy of the analysis was at least 10% and usually better than 2% based on material balance.

Mixtures of H_2S , CO_2 , and H_2O were separated on a 6' X 1/8" column of chromosorb 103 80/100 mesh at 90°C. The helium flow was 75 ml/min.

The various minerals that were tested were NBS standard minerals,* except for the calcite which was purchased from Fisher Scientific.

*We wish to thank Dr. J. C. Butler, chairperson of the Department of Geology, University of Houston, who gave us the minerals.

3.0 MATHEMATICAL ANALYSIS

The rate of the reaction \bar{r} can be estimated using the relation:

$$\bar{r}_i = \frac{q(W_0 - W_i)}{W_s W_0} = \alpha \frac{q P_i}{W_s W_0} \quad (8)$$

where q is the carrier rate of flow, W_s the weight of material in the reactor, W_0 the number of moles that were injected in a pulse, W_i the number of moles of unreacted products, P_i the number of moles of products, and α a stoichiometric coefficient.

The rate of consumption of the solid in the reactor depends on the amount of solid, A , and on the instantaneous concentration of gas, C , around it; several cases deserve special attention and will be discussed in detail. Extension of the theory to other cases is straight forward.

3.1 Rate of Reaction Depends on n -Power of the Solid

When the rate of reaction depends on the n -th power of the weight of the solid in the reactor, A , then:*

$$-\frac{dA}{dt} = kA^n C \quad (9)$$

It is assumed for the moment that only one reaction takes place. If we multiply equation (9) by q , the volumetric rate of flow of the gas, and rearrange the equation we obtain:

$$-\frac{q}{1-n} d(A^{1-n}) = kqC \cdot dt \quad (10)$$

Integration of the equation for the i -th pulse yields

$$-\frac{q}{1-n} (A_i^{1-n} - A_{i-1}^{1-n}) = \int_{t_i}^{\infty} kqC_i dt \quad (11)$$

If the reaction is isothermal and only a small fraction of the pulse is consumed, thus the lower bound on k , k_1 , can be obtained by taking $c = c$ (feed)

$$\int_{t_i}^{\infty} k_1 q c dt = k_1 \int_{t_i}^{\infty} q c_i dt = k_1 W_i \quad (12)$$

where W_i is the number of moles of H_2S that were injected in the i -th pulse. Combining the last two equations yields:

$$\frac{A_i}{A_{i-1}} = \left[1 - \frac{(1-n)k_1 W_i}{q A_{i-1}^{1-n}} \right]^{\frac{1}{1-n}} \quad (13)$$

*This assumption is equivalent to saying that the rate of the reaction depends on a property of the solid which depends on the n -th power of its weight e.g., the surface area is roughly proportional to $A^2/3$.

If $A_i \approx A_{i-1} \approx A_0$ and $W_i = W = \text{constant}$ for all i -s then

$$\frac{A_i}{A_0} \approx \left[1 - \frac{B}{A_0^{1-n}} \right]^{\frac{i}{1-n}} \quad (14)$$

where $B = \frac{(1-n)k_1W}{q}$ (15)

Equation 14 can be used to evaluate B from which the rate constant k can be determined.

When a small fraction of the material is converted, $A_i \approx A_0$, a plot of $\log \frac{A_i}{A_0}$ vs. i yields a straight line with the slope $\frac{1}{1-n} \log \left(1 - \frac{B}{A_0^{1-n}} \right)$. To evaluate n , several experiments should be carried out with different initial amounts of the solid A_0 , or with pulses with a different size, W .

The upper bound on the rate constant k , k_u , can be estimated using the value of c at the outlet:

$$c = \frac{qC_0}{q + \alpha k A^n} \quad (16)$$

where C_0 denotes the concentration of the gas in the feed; and α is a coefficient to account for differences in the stoichiometry. Substitution of equation (16) in equation (9) yields:

$$\frac{q}{k_u(1-n)} (A_i^{1-n} - A_{i-1}^{1-n}) + \alpha (A_i - A_{i-1}) = -W_i \quad (18)$$

From stoichiometry:

$$\alpha (A_{i-1} - A_i) = (W_i - W_{iout}) \quad (19)$$

Therefore:

$$\frac{q}{k_u(1-n)} (A_i^{1-n} - A_{i-1}^{1-n}) = -W_{iout} \quad (20)$$

or

$$\frac{A_i}{A_{i-1}} = \left[1 - \frac{k_u(1-n)W_{iout}}{q A_{i-1}^{1-n}} \right]^{\frac{1}{1-n}} \quad (21)$$

A very important special case is when $n = \frac{2}{3}$. This occurs when the rate of reaction depends on the available surface area. When the solid is "infinitely porous" it may be 1. The case where $n \neq 1$ in the following section.

3.2 Rate of Reaction Proportional to the Weight of the Solid

If all the amount of the solid in the reactor is equally available for reaction, the rate may depend on the first power of the weight of the solid.

$$-\frac{dA}{dt} = kAC \quad (22)$$

The lower bound on the rate constant can be evaluated from the equation:

$$\ln \frac{A_i}{A_{i-1}} = -\frac{k_1}{q} W_i \quad (23)$$

Equation (23) can be simplified if the size of the pulses is equal, namely $W_i = W$ for all i . Then:

$$\frac{A_i}{A_0} = e^{-\frac{k_e W}{q} i} = e^{-\gamma i} \quad (24)$$

$$\gamma = \frac{k_e W}{q} \quad (25)$$

A plot of $\log \frac{A_i}{A_0}$ vs. i should yield a straight line with the slope γ , when such a model holds.

The upper bound on k , k_u , can be evaluated using the equation:

$$\frac{A_i}{A_{i-1}} = e^{-\frac{k_u W_i}{q}} \quad (26)$$

or

$$\frac{A_i}{A_0} = e^{-\frac{k_u}{q} \sum_0^i W_i} \quad (27)$$

3.3 Evaluation of the Rate Constants from Experimental Data

The data that are derived in each experiment include the initial condition of the sample, its weight, W_c , and its specific surface area, S_a . The length of the cycle, θ_c is usually determined by the difficulty of the separation of the products. The number of moles of reactive gas per injection, W , is determined by the fineness of the resolution which is required or by the sensitivity of the experimental system. The value of q can be used to modify B or γ , however it is usually dictated by the separation procedure.

The area of the pulse of gas when no reaction occurs is denoted by S_0 . The area of the peak of unreacted gas from the i -th pulse is denoted by S_i , and the area of the peak of the i -th product from the i -th pulse is denoted by K_i , where the response to the pulsed gas is taken as a unity. The total weight of solid in the reactor can react with the stoichiometric

amount of gas, W_g ; the equivalent area that a peak of magnitude W_g would have had it denoted by S_T . It is assumed that the detectors are linear, therefore, when all the weight of the solid is available for the reaction:

$$\phi_i = \frac{A_i}{A_0} = 1 - i \frac{S_0}{S_T} + \frac{\sum S_i}{S_T} \quad (28)$$

The average rate of consumption of gas per unit mass of solid is:

$$\bar{r}_i = \frac{q(S_0 - S_i)}{W_s S_0} \quad (29)$$

The rate of the single reaction which produces the j -th product is:

$$\bar{r}_i = \alpha \frac{q S_{ji}}{K_j S_0 W_s} \quad (30)$$

Note that if only part of solid, e.g. only a surface layer on the top of each crystal reacts, then S_T will have to be determined experimentally from the relation:

$$S_T = \sum_{i=1}^{\infty} (S_0 - S_i) \quad (31)$$

4.0 RESULTS

The most important variables that affect the rate of the consumption of H_2S are the temperature, the time-temperature history of the sample, the initial conditions of the sample, and the conversion.

Two types of kinetic experiments were conducted: (1) "isothermal," and (2) "temperature programmed." In each experiment, pulses of H_2S with a fixed size were injected, and the amounts of CO_2 , H_2O and unreacted H_2S were determined. In addition, the raw carbonates were tested by DTA and their specific surface area was determined by N_2 adsorption.

Arguments of material balance can be used to deduce the following conclusions: (1) The total number of moles of MS that are formed is equal to the total number of moles of H_2S that are consumed; and also to the number of moles of water that are produced. (2) The number of moles of H_2O and of CO_2 that are produced in reaction 1 as a result of a given pulse of H_2S , is equal to the number of moles of H_2S that are consumed in the reaction. The number of moles of H_2O , in excess to the number of moles of CO_2 , are formed by reaction 3. Figure 3 shows the isothermal rate of consumption of H_2S by calcite, pure dolomite, dolomite, montmorillonite, and sidrite at $570^\circ C$, as a function of the conversion of the solid. The rate of the reaction with H_2S behaves according to one of three modes: (1) rate independent of the conversion, (2) rate decreasing with the conversion, but complete conversion is obtainable, (3) rate decreasing very rapidly with the conversion, and complete conversion is not obtainable.

The rate of reaction of dolomite at 570°C as a function of the conversion is almost constant. However, at 700°C the rate decreases slowly with the conversion. The rate of reaction of calcite at 570°C decreases very sharply, and becomes essentially zero after about 2.8% of the material are converted. At 700°C the rates of conversion of dolomite and calcite to MS are the same.

Sidrite decomposes at much lower temperatures than CaCO_3 or dolomite, FeO and CO_2 are formed. The decomposition of sidrite is complete at 495°C, FeO sinters much more rapidly than CaO . Thus the available surface area of FeO decreases when the sidrite is heated for prolonged times above 500°C. Figure 4 shows the rate of consumption of H_2S by decomposed sidrite that was kept 2-1/4 and 5-1/4 hours at 635°C.

Figure 5 shows the rate of consumption of H_2S by calcite, dolomite, and sidrite which temperature was increased at about 3.3 °C/min. The data were not corrected for the conversion of the material; the effect of the correction is more important at the higher temperatures. The rate of consumption of H_2S by calcite and dolomite seems to be very similar above 650°C, however, different rates are observed below 650°C. Figure 6 shows the rate of evolution of CO_2 from calcite and dolomite as a result of reaction 1. The data show very clearly that the rate of evolution of CO_2 from calcite decreases with the temperature up to 635°C but then it increases very rapidly and at about 700°C it becomes identical to the rate of evolution of CO_2 from dolomite. The rate of evolution of CO_2 from dolomite increases monotonically with the temperature. It should however be noted that the apparent decrease in the rate is due to the coverage of the surface by CaS and the creation of resistance to mass transfer of CO_2 . (The plotted rate is not the initial rate of reaction of clean surfaces). The rate of evolution of CO_2 that results from the thermal decomposition of the carbonate, shows a continuous drift in the detector base line. The decomposition of calcite and dolomite to CaO were complete at 810°C and the decomposition of sidrite was complete at 495°C. Figure 7 shows the rate of formation of water by reaction 3. The data show that the rate of evolution of water becomes almost constant at temperatures above 685°C where no more CO_2 is formed by reaction 1.

5.0 DISCUSSION OF THE RESULTS

The discussion is divided into two parts: discussion of the mechanism of the reactions, and discussion of the rates of the reactions.

5.1 The Mechanism of the Reactions

The rate of consumption of H_2S is influenced by the rates of reactions 1-4, which takes place simultaneously, and by the rate of mass transfer of H_2S , H_2O , and CO_2 through the layer of product MS which is formed on the surface of the MCO_3 crystals. The rate of the chemical reactions is a strong function of the temperature, therefore, different reactions may dominate at different temperatures. In particular, the rate of decomposition of CaCO_3 and of dolomite (reaction 2) becomes very large at temperatures above 739°C. Therefore, large amounts of MO are produced

which competes with the MCO_3 on the available H_2S . Since CaO reacts with H_2S more rapidly than CaCO_3 , the apparent rate of consumption of H_2S by the mixture of CaO-CaCO_3 at temperatures above 730°C is significantly larger than at lower temperatures. Mass transfer in the gas may also become the limiting step at very high temperatures.

The rate of mass transfer in the solid may limit the apparent rate of reaction by preventing the reagent H_2S from reaching the reaction metered, or by preventing the products CO_2 and H_2O from escaping out. The role that the product MS plays depends on the crystalline structure of MS and that of "host" crystal, the MO or the MCO_3 . If the crystalline structures of MS and the host are "compatible" so that the layer of MS can adhere to the surface of the host, (as a solid solution) then resistance to mass transport will be created as a result of the reaction.

Figure 3 shows that at 570°C calcite stops to react after about 2.8 Wt. % of the -200 mesh material was converted. Dolomite, which has the same crystalline configuration continues to react although the initial rate of the reaction depends on the impurities in the material. Dolomite and calcite have the same crystalline structure, except that in dolomite every alternate Ca^{+2} ion is replaced by a Mg^{+2} ion. Had all the components of dolomite been reactive, one would expect that MgS and CaS will be formed as a result of the reactions with H_2S . However, at 570°C only CaS is formed since MgCO_3 does not react with H_2S at 570°C . Therefore, a continuous layer of CaS can not be formed on the surface of dolomite but it can be formed on the surface of calcite. Therefore, once a layer of average thickness of about 7.8 molecules is formed on the surface of the calcite, at least one of the gases CO_2 , H_2O , or CO_2 can not diffuse through it anymore and reaction 1 stops.

It is plausible that the reaction between H_2S and calcite stops because CO_2 cannot diffuse through a layer of CaS . One evidence which supports this theory is that CaO reacts with H_2S according to reaction 3 and is completely converted to CaS . Had CaS been impermeable to H_2O or to H_2S , the reaction of CaO should have also stopped before complete conversion to CaS .

The latter theory is supported by the experimental evidence of CO_2 by retention 1 and of the absorption of H_2S by reactions 1 and 3 as a function of the temperature. The experiment was conducted as follows: first the surface of the calcite was reacted with H_2S at 590°C until the reaction stopped, and then the temperature was programmed up slowly while injecting small pulses of H_2S to study the reactivity of the material. The data shows clearly that around 640°C the layer of CaS breaks, new surfaces of $\text{CaO} + \text{CaCO}_3$ are exposed and reactions 1 and 3 can commence. The equilibrium pressure of CO_2 at 640°C is estimated to be about 0.02 atms. Such a pressure is apparently sufficiently large and can break the layer of CaS .

The crystalline structures of FeO and FeS are different and apparently FeS does not adhere to the surface of FeO . Indeed, even if it adheres,

FeS seems to permit diffusion of H₂S since reaction 3 can proceed at 570°C into completion. However, limited resistance to mass transfer is observed when 3-4 Wt. % of the material is converted.

FeO sinters at a much larger rate than CaO, and at high temperatures its available surface area decreases very rapidly with time. Figure 8 shows that at 570°C, equation (14) with $n = 2/3$ fits the data very adequately, but at 635°C or 700°C the description is inadequate. Equation (14) was derived from equation (9) in which the sintering effect which reduces the surface area was not taken into consideration. Note that an increase in the temperature results in an increase in the rate constant of reactions 3 and 4. The latter reaction reduces the surface area which is available for reaction with H₂S according to reactions 1 and 3.

5.2 Quantitative Rate Data

Rate data on some selected systems is presented in Table 2. The data were derived on samples of particles -200 mesh, of about 0.1-0.2 gm each. Unless otherwise specified, the material was permitted to equilibrate 2-1/4 hours at the reaction temperature. Equation (14) with $n = 2/3$ has been used to evaluate the lower bound on the rate constant.

The evaluation of the activation energies and their use should be done with caution, since they have greatly different values in different temperature regions. A summary of the data is given in Table 2.

TABLE 2
Activation Energies for the Rate of Consumption
of H₂S by Minerals

| <u>Material</u> | <u>T°C Range</u> | <u>Controlling Mechanism</u> | <u>Ea kcal/mole</u> ±30% |
|--|------------------|---|-----------------------------|
| Calcite | 560 | Diffusion of gas through CaS | 0.0 |
| Calcite (with CaO) | 560-670 | Rate of reaction | 19.0 |
| Calcite (with CaO) | 670 | Rate of gas-phase mass transfer | 4.0 |
| Dolomite | 640 | Rate of reaction | 12.2-13.5 |
| Dolomite (with CaO-MgCO ₃) | 640 | Rate of gas-phase mass transfer | 2.4 |
| Sidrite (with FeO) | 460 | Rate of reaction | 15.2 |
| FeO | 460 | Rate of gas-phase + mass transfer and sintering | 0.0 |

In general, mass transfer controls when the reacting material is a carbonate, and the rate of reaction (2) or the rate of gas-phase mass transfer will control when the reacting solid is the oxide. Small activation energies (0-4 kcal/mole) are observed when the carbonate reacts and 30-45 kcal/mole are observed when the oxide reacts. Note should however be made of the decomposition reaction 2 in which the carbonate is transformed into an oxide. This reaction can not be controlled and it tends to activate the solid even when the carrier gas contains CO₂ (the rate of reaction 2 is suppressed in the latter case).

REFERENCES

- Armstrong, V. and Himms, G. W., Chem. and Ind., June 10, 543 (1939).
- Attar, A., "The Fundamental Chemistry and Modeling of the Reactions of Sulfur in Coal Pyrolysis," Paper presented in the AIChE Meeting, Houston, Texas, March 1977.
- Attar, A., "The Fundamental Chemistry and Modeling of the Reactions of Sulfur in Coal Pyrolysis and Hydrogenation," In print in a Chemical Engineering Progress technical manual.
- Bertrand, M. F., "Gas Purifying Materials," Brit. Pat., 462, 934 (1937). C.A. 31-6446.
- Bragg, L. and Claringbull, G. F., "Crystal Structures of Minerals," Cornell University Press, Ithaca, N. Y. (1965).
- Gluud, W., Keller, K., Klempt, W., and Berthorn, R., "Development and Operation of a New Process for Hydrogen and Hydrogen-Nitrogen Mixtures," Ber. Ges. Kohlentech., 3, 211 (1930).
- Greenwood, N. N., "Ionic Crystals, Lattice Defects and Nonstoichiometry," Butterworths, London (1970).
- Parks, G. D., "Mellons Modern Inorganic Chemistry," Longmans, London (1961).
- Powell, A. R., Ind. Eng. Chem., 13, 33 (1921).
- Ruth, L. A., Squires, A. M., and Graft, R. A., "Desulfurization of Fuels with Calcined Dolomite," Paper presented in the ACS Meeting, Los Angeles, California, March (1971).
- Squires, A. M., "New Systems for Clean Power," Int. J. Sulfur Chem., Part B, 7 (1), 85 (1972).
- Stinnes, G. M., "Gas Purifying Materials," Brit. Pat., 371, 117 (1930). C.A. 27-2565.
- Thiessen, G., "Forms of Sulfur in Coal," Chapt. 12, p. 475 in "Chemistry of Coal Utilization," Lowry, H. H., (ed.), Wiley, N. Y. (1945).

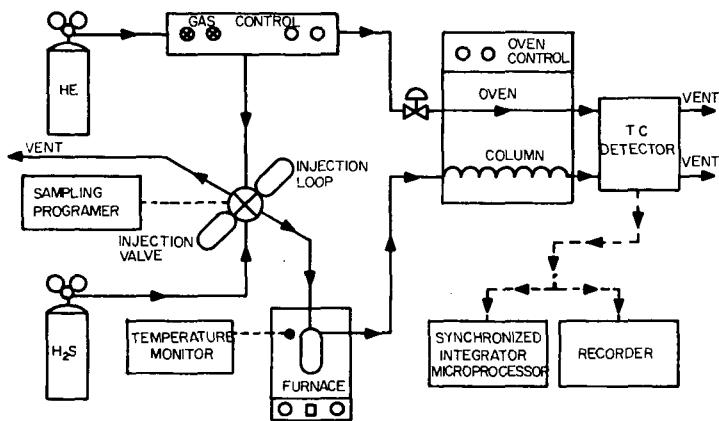


FIGURE 1: SCHEMATIC DIAGRAM OF EXPERIMENTAL SYSTEM

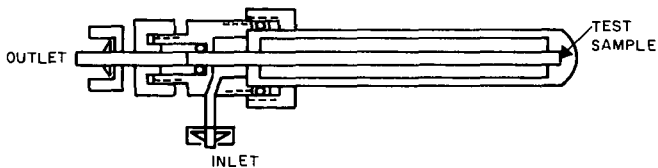


FIGURE 2: CROSS SECTION OF THE HIGH TEMPERATURES MICRO-DIFFERENTIAL REACTOR.

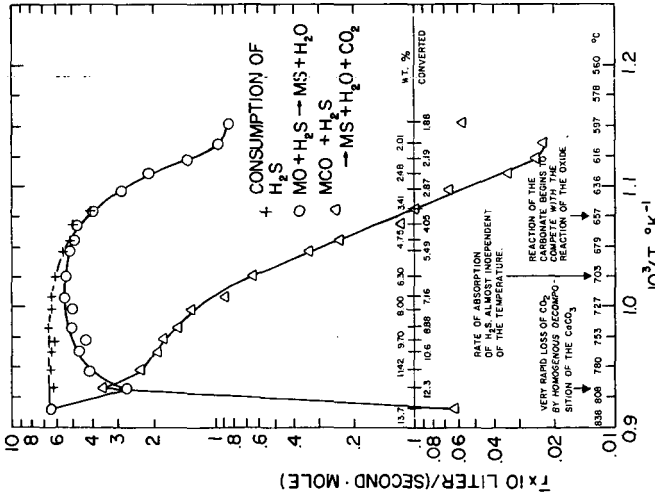


FIGURE 7: RATE OF CONSUMPTION OF H₂S AND THE RATES OF EVOLUTION OF H₂O AND CO₂ AS THE TEMPERATURE WAS PROGRAMMED UP AFTER THE REACTION AT 590°C STOPPED. SEE TEXT.

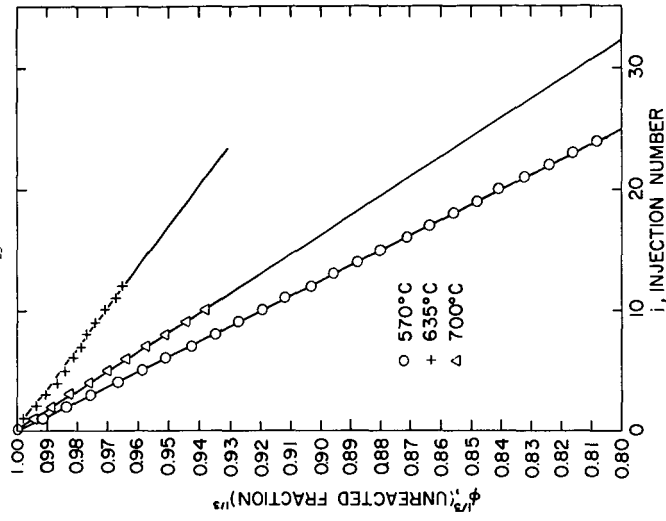


FIGURE 8: THE PROGRESS OF THE REACTION OF SIDRITE AT DIFFERENT TEMPERATURES.

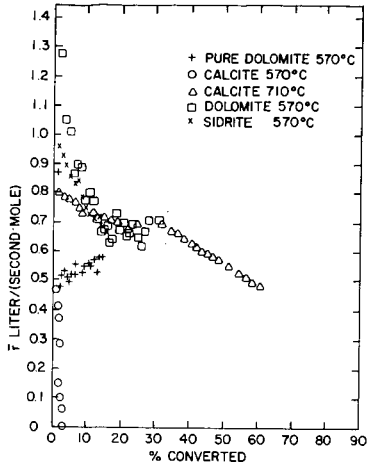


FIGURE 3: THE RATE OF CONSUMPTION OF H_2S BY BASIC MINERALS.

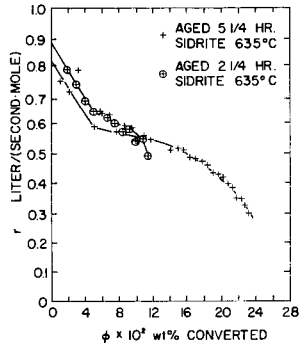


FIGURE 4: THE RATE OF CONSUMPTION OF H_2S BY DECOMPOSED -200 MESH SIDRITE AT $635^\circ C$

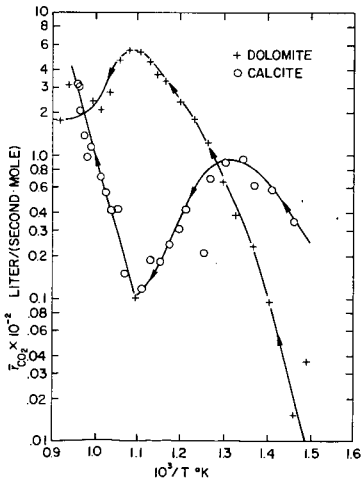


FIGURE 6: RATE OF EVOLUTION OF CO_2 FROM CALCITE AND DOLOMITE IN A TEMPERATURE-PROGRAMMED TEST.

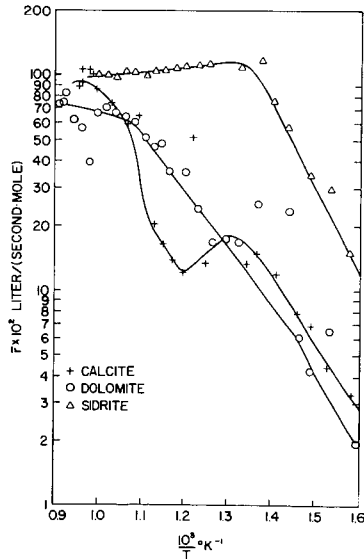


FIGURE 5: THE VARIATION IN THE RATE OF CONSUMPTION AT H_2S BY BASIC MINERALS IN TEMPERATURE PROGRAMMED EXPERIMENTS.

IDENTIFICATION OF ISOPRENOIDS, STERANES, AND
TERPANES IN FISCHER ASSAY RETORTED SHALE OILS

J. Renzo Morandi and Frank Guffey

Department of Energy
Laramie Energy Research Center
P. O. Box 3395
Laramie, Wyoming 82071

INTRODUCTION

In the past 15 years much work has been done on the identification of individual compounds in the branched-plus-cyclic paraffin hydrocarbon fractions from Green River oil shale bitumens; i.e., on the small amount of material that can be solvent extracted from the shale. Cummins and Robinson (1) identified the C-16, C-18, C-19, and C-20 isoprenoid alkanes. Burlingame and coworkers (2) reported the presence of C-27, C-28, and C-29 steranes. Eglinton and coworkers (3) identified cholestane, ergostane, sitostane, and perhydro- β -carotene. Anders and Robinson (4) identified 52 cyclic alkanes, and Henderson (5) identified steranes and triterpanes. Gallegos (6) identified 36 individual components in the saturate fraction of an oil shale bitumen. Robinson and Cook (7) studied the bitumen from a Wyoming oil shale core with respect to the variations in the distribution of various alkanes with stratigraphy.

Most of the geochemical studies have been made on the unpyrolyzed bitumen because of the suspicion that pyrolysis of the kerogen would destroy or alter the biological markers and thus negate the results. However, recent studies suggest that some of these markers survive pyrolysis. Gallegos (8) reported the presence of gammacerane and the C-27, C-28, and C-29 steranes in a pyrolysis study of so-called "kerogen-shale"--shale residue after the extraction of solubles with a benzene-methanol mixture. Takeo (9) reported the presence of C-18 and C-20 alkane isoprenoids in an N.T.U. shale-oil distillate.

In this study, saturate fractions of Fischer assay oils from an earlier study (10) were examined in detail to see if the biological markers survive the retorting process. A study of these biological markers in the oils produced from a core might be used as an aid in the geochemical study of sediments. Although this core is not identical to that studied by Robinson and Cook, it is from the same area so that some comparisons can be made between the bitumen and the pyrolyzed product.

EXPERIMENTAL

A core was obtained from northern Green River Basin in T21N, R107W, Sweetwater County, near Rock Springs, Wyoming. Fischer assay (11) was carried out on the sections of the core containing kerogen. A lithographic description of the core was used to composite the Fischer assay oils into 11 composite oils comprising the oil produced from adjacent shale seams of similar appearance. The 11 composite oils are representative of the three principal members of the Green River oil shale formation in this basin. The first two composite oils, L-1 and L-2, are from the Laney member; the next eight composite oils, WP-1 to WP-8, are from the Wilkins Peak member; and the last oil, T-1, is from the Tipton member, which is the lowest stratum containing kerogen.

A saturate fraction of each composite oil was prepared by dissolving 3 g of oil in approximately 10 ml of cyclohexane. The nonsaturates were removed by sulfonation and centrifugation as described in ASTM method D-1019 (12). The resulting cyclohexane-saturates solution was chromatographed on a 1/2-in. i.d. by

6-in. column packed with 60-200 mesh silica gel and eluted with benzene. Organic material was recovered by rotary evaporation of solvent.

Each saturate fraction was separated into n-paraffins and branched-plus-cyclic paraffins (BCP) by molecular sieves. The n-paraffins were recovered by destroying the molecular sieves with hydrofluoric acid (13).

All the n-paraffins and BCP fractions were analyzed using a Hewlett-Packard* 5710A gas chromatograph equipped with a flame ionization detector. Paired 50-ft by 0.02-in. i.d. support coated open tubular (SCOT) columns coated with Dexsil 300 were used. The chromatograph was programmed from 100°C at 4° per minute up to 300°C, where the temperature was maintained for 16 minutes.

Combined gas chromatography-mass spectrometry (GC-MS) of selected samples were obtained using a Hewlett-Packard 5710A gas chromatograph and an AE IMS-12 mass spectrometer. A similar SCOT column was coupled directly to the source of the MS-12 without the benefit of a separator. All the mass spectra were obtained at 70 volts.

Data acquisition and processing were accomplished with a Finigan Incos 2300 series mass spectrometer data system. The magnet cycle time was 18 seconds.

RESULTS AND DISCUSSION

Geochemical investigations of biological markers are usually made on samples that have been carefully collected and preserved to prevent the formation of artifacts. However, recent work by Gallegos (8) suggests that some of the biological markers survive the retorting process, and Gallegos suggests that "The terpanes which have survived pyrolysis rather than those extracted reflect more faithfully the distribution and identity of the terpanoids originally laid down in the sediments." To investigate these possibilities, we examined the alkane hydrocarbons in oils produced by retorting oil shales from different geologic regimes. All the shales were retorted in identical fashions by Fischer assay which heats the shale at a controlled rate to 500°C.

Geology

A brief description of the geology of the area from which the subject core was obtained will set the stage for the discussions. The oil shales of the Green River Formation in Wyoming were formed in Gosiute Lake in early and middle Eocene age (14). This lake went through three major changes in size. During the first stage, in which the Tipton member was laid down, it was large and overflowing, and thus a fresh water lake. During the second, or Wilkins Peak stage, the lake shrank and became extremely saline. When the top, or Laney member, was laid down the lake had again expanded, overflowed, and become a fresh water lake.

General Characteristics

Table 1 shows the depth and length of the sections that were composited for Fischer assay, together with the oil yield, the percent of total saturates, and the percents of this saturate fraction that are normal and branched-plus-cyclic paraffins (BCP). The lengths of the core vary from 193 feet for WP-6 to 7 feet for T-1, showing considerable difference in the length of the homogeneous bands. The oil yield data show that the oil shale in this area is lean, ranging from 4.5 to 15.9 gallons per ton. The average yield for the core, excluding the barren sections, (most of which are in the top 300 feet) is 9.0 gallons per ton. The

*Mention of specific brand names or models of equipment is for information only and does not constitute an endorsement by the Department of Energy.

saturates represent 9 to 11 percent of all the oils except the Tipton, the single sample of which has a somewhat higher saturate content than the other oils. A previous study (10) showed that the Tipton oil had significantly smaller amounts of polar compounds than the other oils. Thus, its high content of paraffins may simply reflect a lack of dilution by the polar components.

TABLE 1. - Description of Wyoming core and percentages of saturates, normal, and branched-plus-cyclic hydrocarbons in the Fischer assay oils

| Section ^{1/} | Depth ^{1/} ft. | Length ^{2/} ft. | Yield, gal/ton | Saturates, vol. % of oil | Vol % of saturates | |
|-----------------------|----------------------------|-----------------------------|-------------------|--------------------------------|--------------------|------------------------------|
| | | | | | n-paraffins | Branched-cyclic paraffins |
| L-1 | 771.5 | 38.1 | 5.3 | 9.7 | 63.9 | 36.1 |
| L-2 | 870.5 | 59.6 | 10.3 | 11.1 | 60.4 | 39.6 |
| WP-1 | 1064.7 | 44.3 | 13.5 | 8.9 | 39.3 | 60.7 |
| WP-2 | 1109.0 | 48.6 | 15.1 | 9.7 | 46.4 | 53.6 |
| WP-3 | 1157.6 ^{4/} | 41.2 | 11.0 | 10.2 | 45.1 | 54.9 |
| WP-4 | 1250.0 ^{4/} | 26.4 | 8.0 | 9.8 | 48.0 | 52.0 |
| WP-5 | 1276.4 | 45.6 | 15.9 | 9.7 | 51.5 | 48.5 |
| WP-6 | 1322.0 | 193.0 | 6.1 | 9.9 | 39.4 | 60.6 |
| WP-7 | 1515.0 | 101.0 | 8.9 | 9.8 | 51.0 | 49 |
| WP-8 | 1616.0 | 94.0 | 7.3 | 10.0 | 56 | 44 |
| T-1 | 1710.0 | 7.0 | 4.5 | 13.3 | 63.9 | 36.1 |

^{1/} L = Laney member, WP = Wilkins Peak member, T = Tipton member

^{2/} Top of section

^{3/} Excluding barren section

^{4/} 51.2 feet of core missing between WP-3 and WP-4

Normal Paraffins

Table 1 shows variations in the composition of the saturate fractions with regard to their content of n-paraffins. The Laney and Tipton saturates are 60 to 64 percent n-paraffin, while the Wilkins Peak saturates contain significantly lower amounts. Thus, the two freshwater deposits are higher in n-paraffins than the saline deposit. The high value of WP-8, which is adjacent to the Tipton core, may suggest an influence of the freshwater member on its adjacent saline member; i.e., a somewhat gradual transition from fresh to saline.

Gas chromatographic investigation of the n-paraffin fractions of the 11 oils shows n-paraffins from C-11 to C-34 with the greatest abundance at about C-17. The odd-to-even preference that was noted in n-paraffin fractions of bitumens from a similar core (7) is absent. This result was not unexpected in these oils, which had been heated at 500°C, because Cummins (15) showed disappearance of the odd-to-even preference when shales were degraded at temperatures of 150 to 350°C.

Branched-Plus-Cyclic Paraffins

Gas chromatograms of the BCP fraction of the oils suggested the presence of chain isoprenoids, steranes, and pentacyclic triterpanes. Chromatograms of samples from each of the members are shown in Figure 1. Combined GC-MS analyses were obtained on these three representative fractions to identify the major peaks. An example of the resulting reconstructed chromatograph for the Wilkins Peak sample is shown in Figure 2. Two of the peaks--26 and 31--contained two compounds, while each of the others contained one. Thirty-six compounds were identified in the GC

fractions and accounts for 55 percent of the BCP fraction. In several instances, as will be noted later, the MS identification was confirmed by coinjection of authentic samples. The qualitative data from the mass spectra may now be combined with the quantitative data from gas chromatography to examine the various types of compounds that are present in these oils.

Chain isoprenoids. - The larger peaks in the first part of the gas chromatograms (Figure 1) are chain isoprenoids. The GC peak number and the empirical formula of these compounds are listed in Table 2. The gas chromatographic data in Figure 1 show considerable variation in the amounts of the individual isoprenoids. Phytane (peak 14) increases from 2 percent in the Tipton to 5.5 in the Wilkins Peak and to 8.3 in the Laney. This increase in a compound usually thought to be a degradation product of chlorophyll (4) may suggest an increase in the amount of vegetative matter as the lake went from the Tipton to Wilkins Peak to Laney.

TABLE 2. - Chain isoprenoids ($C_{n-2}H_{2n+2}$) identified

| GC peak no. | Empirical formula | Molecular weight | Common name |
|-------------|-------------------|------------------|-------------|
| 1 | $C_{13}H_{28}$ | 184 | |
| 2 | $C_{14}H_{30}$ | 198 | |
| 4 | $C_{15}H_{32}$ | 212 | Farnasane |
| 6 | $C_{16}H_{34}$ | 226 | |
| 8 | $C_{17}H_{36}$ | 240 | |
| 10 | $C_{18}H_{38}$ | 254 | |
| 12 | $C_{19}H_{40}$ | 268 | Pristane |
| 14 | $C_{20}H_{42}$ | 282 | Phytane |
| 15 | $C_{21}H_{44}$ | 296 | |
| 15A | $C_{22}H_{46}$ | 310 | |
| 16 | $C_{23}H_{48}$ | 324 | |
| 17 | $C_{24}H_{50}$ | 338 | |
| 18 | $C_{25}H_{52}$ | 352 | |
| 19 | $C_{30}H_{62}$ | 412 | Squalane |

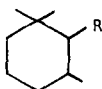
Inspection of Figure 1 reveals many differences in the ratios of the amounts of the chain isoprenoids. For example, the ratio of the heights of peaks 10, 12, and 14 changes from 1.2/1.0/2.4 to 1.2/1.0/1.3 to 0.8/1.0/1.0 as the depth increases.

Monocyclic Isoprenoids. - Eight monocyclic isoprenoids shown in Table 3 were identified, These are the small, odd-numbered peaks in the first part of the chro-

TABLE 3. - Monocyclic isoprenoids (C_nH_{2n}) identified

| GC peak no. | Empirical formula | Molecular weight |
|-------------|---------------------------------|------------------|
| 3 | C ₁₄ H ₂₈ | 196 |
| 5 | C ₁₅ H ₃₀ | 210 |
| 7 | C ₁₆ H ₃₂ | 224 |
| 9 | C ₁₇ H ₃₄ | 238 |
| 11 | C ₁₈ H ₃₆ | 252 |
| 13 | C ₁₉ H ₃₈ | 266 |
| 18A | C ₂₉ H ₅₈ | 406 |
| 32 | C ₄₀ H ₇₈ | 558 |

matograms (Figure 1) and 18A in the chromatogram of T-1. These compounds have the empirical formula C_nH_{2n}, and the general structure



where R is a saturated chain of varying length. The amounts of these compounds, which are thought to be derived from perhydro-β-carotene, are small so that quantitative differences are obscured except for the C-29 compound (peak 18A). This compound makes up 2.3 percent of the BCP fraction of the Tipton but is absent in the Wilkins Peak and the Laney. The mass spectrum of this compound shows fragments that are typical of monocyclic isoprenoids.

Dicyclic Isoprenoid--Perhydro-β-Carotene. - A dicyclic compound, peak 32 in Figure 1, was shown to be perhydro-β-carotene. The parent molecular ion observed in the mass spectrum of this component was at m/g = 558. Diagnostic fragment ions in the spectrum occurred at m/g = 125, 137, and 502. These ions have been noted in the mass spectrum of perhydro-β-carotene (6). The identity of component 32 was verified by coinjection of an authentic sample.

Steranes. - The steranes identified in the BCP fractions of the retorted oils are shown in Table 4. The compounds were identified by comparing mass spectra with published spectra and by coinjection in the case of the two cholestanes. All of these compounds have been identified in shale oil bitumen by Gallegos (6), Eglinton (3), Henderson (5), and others.

TABLE 4. - Sterane ($C_{2n}H_{4n-6}$) compounds identified

| GC peak no. | Empirical formula | Molecular weight | Common name |
|------------------|-------------------|------------------|--------------------------|
| 20 | $C_{27}H_{48}$ | 372 | 5- β -cholestane |
| 21 | $C_{27}H_{48}$ | 372 | 5- α -cholestane |
| 22 | $C_{28}H_{50}$ | 386 | 5- β -ergostane |
| 23 | $C_{28}H_{50}$ | 386 | 5- α -ergostane |
| 24 | $C_{29}H_{52}$ | 400 | 5- β -stigmastane |
| 25 | $C_{29}H_{52}$ | 400 | 5- α -stigmastane |
| 26 ^{1/} | $C_{30}H_{54}$ | 414 | unknown |

^{1/} Peak contains two compounds, one of which is a tetracyclic terpene, the other a pentacyclic triterpene of mass 398

The amounts of these compounds vary greatly, as shown in Figure 1. The Wilkins Peak samples contain more 5- α -ergostane (peak 23) and 5- β -stigmastane (peak 25) than either the Laney or the Tipton samples. A comparison of these peaks in the 11 samples shows three times as much α -ergostane and about four times as much α -stigmastane in the Wilkins Peak samples as in the Laney or Tipton samples. This, again, indicates that the sedimentary deposition during the Wilkins Peak time was different than during the Laney or the Tipton time.

The ratio of the abundance of the 5- α - to the 5- β - isomers of all three steranes--cholestane, ergostane, and stigmastane--was approximately 3 to 1, similar to that found by Gallegos (6) in oil shale bitumen. Thermodynamically, the more stable isomer is the alpha form, and the above results indicate that exposure to 500°C during the retorting step does not change the ratio of the alpha to beta isomers.

Pentacyclic Triterpanes. - The pentacyclic triterpanes identified are listed in Table 5. The structures of these compounds are shown in Figure 3. All of these compounds have been previously identified (4, 6, 7). Peak 26 contains two compounds. One is a pentacyclic triterpene with a molecular weight of 398; the mass spectrum of this compound is similar to the pentacyclic triterpene D reported by Whitehead (16) and by Gallegos (6) as compound 30. The peak labeled 27, Figure 3, is believed to be an isomeric form of the compound that emerged as part of peak 26. It was not possible to determine the position of the methyl group in the E ring of peak 27 from the fragmentation pattern. Peaks 28 and 29 are believed to be isomeric compounds with the structure shown in Figure 3. It was not possible to identify the position of the propyl group in these compounds, one of which may be hopane, as suggested by Henderson (5). Peaks 30 and 31 are apparently isomeric pentacyclic triterpanes, with the structures shown in Figure 3.

TABLE 5. - Pentacyclic triterpanes (C_nH₂₂₋₈) identified

| GC peak no. | Empirical formula | Molecular weight |
|------------------|---------------------------------|------------------|
| 26 ^{1/} | C ₂₉ H ₅₀ | 398 |
| 27 | C ₂₉ H ₅₀ | 398 |
| 28 | C ₃₀ H ₅₂ | 412 |
| 29 | C ₃₀ H ₅₂ | 412 |
| 30 | C ₃₁ H ₅₄ | 426 |
| 31 ^{2/} | C ₃₁ H ₅₄ | 426 |

^{1/} Peak contains two compounds, one of which is a pentacyclic triterpane, the other a tetracyclic terpene with a molecular weight of 414.

^{2/} Peak contains two compounds, one of which is gammacerane, and an unidentified pentacyclic triterpane.

Semi-Quantitative Comparisons

Table 6 presents semi-quantitative data on some of the types of compounds in the BCP fraction. The data were obtained by integrating the areas under the chro-

TABLE 6. C-13 to C-20 chain isoprenoids, α -steranes, and perhydro- β -carotene in the branched-cyclic fraction of the retorted oils

| Section | Vol % in branched-plus-cyclic fraction ^{1/} | | |
|-------------------------------|--|--------------------|-----------------------------|
| | Chain Isoprenoids | α -Steranes | Perhydro- β -carotene |
| L-1 | 16.9 | 2.9 | 0.8 |
| L-2 | 21.0 | 4.9 | 1.3 |
| WP-1 | 17.7 | 8.8 | 1.4 |
| WP-2 | 26.5 | 8.2 | 0.9 |
| WP-3 | 25.2 | 5.2 | 1.0 |
| WP-4 | 25.4 | 8.5 | 0.7 |
| WP-5 | 23.6 | 6.0 | 1.4 |
| WP-6 | 23.0 | 6.7 | 1.2 |
| WP-7 | 20.4 | 8.3 | 1.4 |
| WP-8 | 17.4 | 5.4 | 2.1 |
| T-1 | 10.5 | 2.6 | 0.5 |
| Oil average | 20.7 | 6.1 | 1.1 |
| Bitumen average ^{2/} | 29.9 | 14.1 | 4.6 |

^{1/} Area percentages calculated from FID chromatogram

^{2/} Data from Cook and Robinson (7)

matographic peaks for perhydro- β -carotene and for the C-13 to C-20 compounds listed in Table 2 and the α -steranes in Table 4. The data are semi-quantitative because of the difficulty in establishing a baseline. No attempt was made to integrate the small peaks for monocyclic isoprenoids and β -steranes. In general the table shows lower amounts of chain isoprenoids, α -steranes, and perhydro- β -carotene in the samples from the Laney and the Tipton member than in the Wilkins Peak samples. This suggests that the sedimentary deposition during the Laney and the Tipton time was different than during the highly saline period of the Wilkins Peak time.

Table 6 also shows the average of chain isoprenoids, α -steranes, and perhydro- β -carotene for the 11 oils and a similar calculation on the bitumen samples studied by Robinson and Cook (7). The BCP fraction of the bitumen contains 1.4 times more chain isoprenoids, about twice the amount of α -steranes, and about 4 times more perhydro- β -carotene than the retorted samples.

CONCLUSIONS

Biological markers have been identified in shale oil produced by Fischer as-say retorting of oil shale. The biological markers identified include isoprenoid alkanes, monocyclic terpanes, steranes, and pentacyclic triterpanes. These are the same classes of compounds that have been identified in extracted bitumen and pyrolyzed oil shale. The results from this study do not indicate the source of these compounds in oil shale. These compounds probably represent material from both the bitumen and kerogen.

The distribution of these compounds in the different sedimentary layers varies considerably. The data show little if any influence of depth-related factors, a conclusion similar to that drawn from a study (7) of the bitumen from a Wyoming core. Although the phytane appears to decrease with increasing depth, this may be due to an increase in the amount of vegetative (chlorophyll-bearing) matter as the lake went from the Tipton to the Laney era. In agreement with the bitumen data of Robinson and Cook, we found that the Laney (top) and the Tipton (bottom) member samples were usually similar and had a somewhat lower quantity of isoprenoids, steranes, etc., than the Wilkins Peak (middle) member samples. This difference is probably due to the differences in environment, that is, fresh water lake during the Laney and Tipton eras and a salt water lake during the Wilkins Peak era.

The chain isoprenoid content in the BCP fractions from the 11 retorted oils average approximately 21 percent, and Robinson and Cook's results for the bitumen on their core were about 30 percent. Although direct comparisons cannot be made because their work was on a different core and on the extracts of the oil shale from the core, our results appear to indicate that the chain isoprenoids are stable to the retorting process. The chain isoprenoids averaged approximately 19 percent for the Laney, 23 percent for the Wilkins Peak, and 10 percent for the Tipton samples. This difference in the amount of these isoprenoids in the three member samples points out again the difference in the environment in the Gosiute Lake during the formation of these three members.

For the most part, previous studies of the biological markers in oil shale have dealt with the material extracted from bitumen. Gallegos had indicated that the material produced from the pyrolysis of oil shale may be more indicative of the biological source material than extracted bitumen (6). We feel that both the material from extracted bitumen and the product oil should be investigated for a more complete geochemical picture of oil shale formation.

REFERENCES

1. J. J. Cummins and W. E. Robinson, *J. Chem. Eng. Data*, 9, 304 (1964).
2. A. L. Burlingame, P. Haug, T. Belsky, and M. Calvin, *Proc. Nat. Acad. Sci.*, 54, 1406 (1965).
3. Sister Mary, T. J. Murphy, A. McCormick, and G. Eglinton, *Science*, 157, 1040 (1967).
4. D. E. Anders and W. E. Robinson, *Geochim. et Cosmochim. Acta*, 35, 661, (1971).
5. W. Henderson, Wojtech Wollrab, and G. Eglinton, *Advances in Org. Geochem.*, 1968, 181.
6. E. J. Gallegos, *Anal. Chem.*, 43, 1151, (1971).
7. W. E. Robinson and G. L. Cook, U.S. BuMines, Rept. of Inv. 7820 (1973).
8. E. J. Gallegos, *Anal. Chem.*, 47, 1524, (1975).
9. Iida Takeo, *Yakugaku Zasshi*, 96, 796, (1976).
10. L. P. Jackson, J. R. Morandi, and R. E. Poulson, Preprints, Div. Fuel Chem., ACS, 22 (3), 66, (1977).
11. K. E. Stanfield and I. C. Frost, U.S. BuMines, Rept. of Inv. 4477 (1949).
12. ASTM Book of Standards, 1975, Part 23, Method D-1019-68, p. 477.
13. J. V. Brunnock, *Anal. Chem.*, 38, 1649, (1966).
14. W. H. Bradley and H. P. Euster, U.S. Geol. Survey Prof. Papers, 496-B, 71 pp. (1969).
15. J. J. Cummins, F. G. Doolittle, and W. E. Robinson, U.S. BuMines Rept. of Inv. 7024 (1974).
16. I. R. Hills and E. V. Whitehead, *Nature*, 209, 977 (1966).

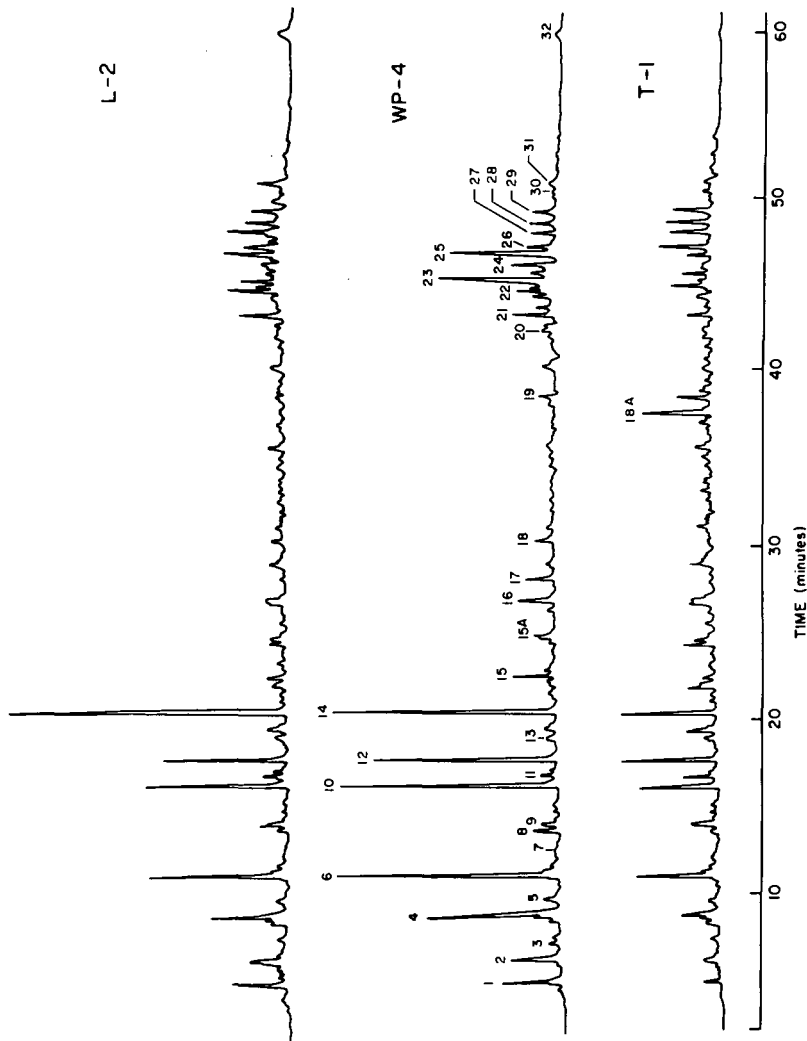


FIG. 1. GAS CHROMATOGRAPHS (FID) OF THE BRANCHED-CYCLE HYDROCARBON FRACTION FROM RETORTED WYOMING SHALE OIL.

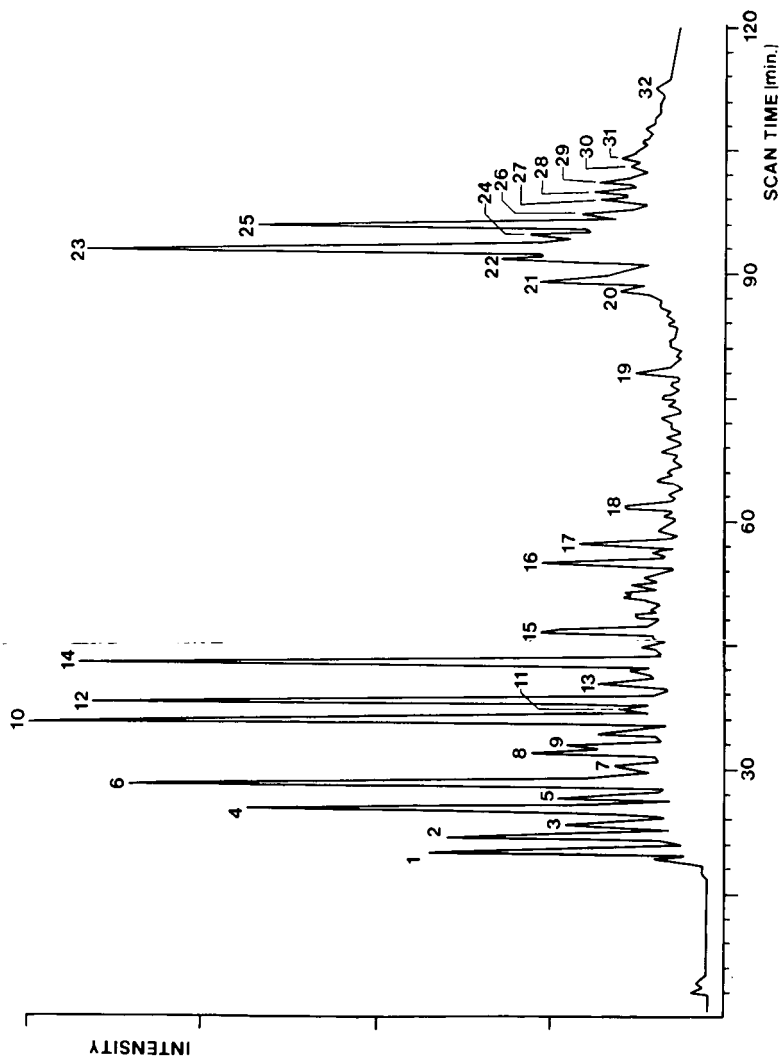
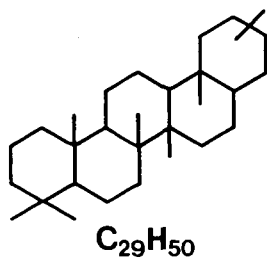
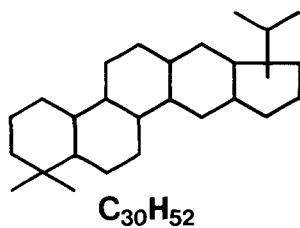


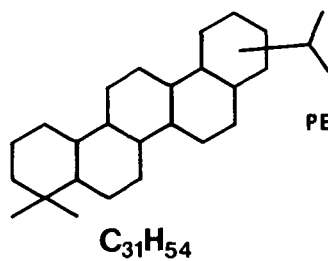
FIG. 2. RECONSTRUCTED GAS CHROMATOGRAPH OF BRANCHED-CYCLE
HYDROCARBON FRACTION FROM WP-4 RETORTED WYOMING SHALE OIL.



PEAK NO. 26 & 27



PEAK NO. 28 & 29



PEAK NO. 30 & 31

FIG. 3. PENTACYCLIC TRITERPANES IN GREEN RIVER RETORTED SHALE OIL

GAS COMPOSITION CALCULATION FOR THE IN SITU
GASIFICATION OF THIN SEAMS AND THE APPROACH TO MODELING

S. Debrand and O. J. Hahn

Institute for Mining and Minerals Research
University of Kentucky
Lexington, Kentucky 40506

INTRODUCTION

The Appalachian region contains numerous coal seams which are under 60 inches in thickness. A portion of this coal is usually recovered by Auger mining techniques after contour stripping. At least fifty percent of the remaining coal may be gasified to produce a low Btu fuel. The application of underground gasification to very thin seams (below 40 inches in thickness) is limited by the reduction of the heating value of the gas. This reduction is caused by an excessive heat loss to the surrounding strata. The purpose of this work was to evaluate the pertinent factors affecting the gas composition and the limitations of modeling calculations. The logical sequences leading to a gas composition model and the estimation of the temperature profile in the gasification zone were presented. The available literature data related to the various calculation techniques were also quoted.

PARAMETERS AFFECTING THE GAS COMPOSITION

The total heat losses during the in situ gasification affect significantly the gas composition and its heating value. A heat balance results in a temperature profile of the gasification zone. One modeling approach is to calculate the gas composition and compare this composition to the data obtained from the experimental tests. A second approach involves a prediction of the temperature profile of the gasification zone. The gasification of coal seams having a thickness from one or more meters is considered here. The combustible gases formed during the underground forward gasification mode are obtained by pyrolytic coal decomposition superimposed upon the gasification products. As far as the gasification is concerned, the reaction of coal with the steam and/or hydrogen is of paramount importance because this is the main reaction which produces a gaseous burnable product of heating value above 100 Btu/SCF. The ratio of the total amount of water (in the form of coal moisture plus inflow of water or steam) to the supplied amount of oxygen seems to be a predominant factor in maximizing gas heating value for the defined level of total heat losses.

In general, the gas composition of the underground gasified coal depends on the volatile content, the seam moisture, the blast air moisture content, and the chemical reactivity of the coke. The gasification efficiency and combustion stability are sensitive [Stewart et al. (24)] to the optimum combination of the coal seam moisture and of blast air moisture.

The reactivity of a particular coal is a function of the chemical properties of its organic and mineral constituents and of the physical structure of the coal; generally, it is observed that the coal reactivity in gasification increases with decreasing coal rank and is proportional to the internal surface area [Schora, F. (23)]. When experimental values for the relative low-rate gasification reactivity factors (f_o) are not available; values for many coal [Johnson, S. L. (15)] may be estimated from the following equation: $f_o = 6.2 y (1-y)$ where y is the mass fraction of total carbon in the original coal on a dry ash-free basis. The conditions during a pyrolysis of the coal affect the physical nature of the char and

its reactivity. In the temperature range 600-700° C, where the apparent activation energy is high (80-70 kcal/mole), the reaction rate is low and the composition of gas is limited by the kinetic reaction rate; in the temperature range 700-750° C the diffusion process through the pore structure is a limiting factor. However, [Limears et al. (19)] have shown that for some coal types the particle size has nearly no effect upon the char reaction rate.

In general, the rate of the steam-hydrogen reaction with the coal depends on many variables such as: temperature, pressure, character of the coal solid surface and the amount of volatile matter in coal. The first stage of the reaction is rapid and is related to the gasification of the carbon portion included in the volatile matter. The low reactivity coal portion is the residual, carbonaceous coke. This stage is usually denoted as (1) $C^* + H_2O \rightarrow CO + H_2$ and (2) $H_2 + H_2O + 2C \rightleftharpoons CO + CH_4$ where C^* is the reactive carbon in the volatile matter. Most coals are made up of a number of macerals which differ in their reactivity. [Davis et al. (19)] found a reactivity order fusian < durain < vitrain.

The endothermic reaction of steam with carbon is of primary importance. These endothermic reactions are maintained by the endothermic oxidation reaction of carbon and oxygen.

The higher activation energy observed for the carbon reaction with the steam-hydrogen mixture indicated an inhibiting effect of hydrogen (and/or methane) on the char-steam reaction. The reactivity of such a mixture was proportional to the steam pressure raised to the 0.93 power [Johnson (15)].

[Young et al. (30)] reported on the effect of the steam upon the methane production and the shift reaction under conditions that are similar to those of underground gasification. Wyodak and Hanna char was used. No carbon monoxide was detected for the steam-char gasification process to indicate that the water shift reaction $CO + H_2O \rightarrow CO_2 + H_2$ had taken place. The gas shift reaction was probably catalyzed by the ash content in the char. Introduction of steam during the pyrolysis period doubled the rate of methane production. The rate of methane production was 20 percent of that of carbon dioxide. Russian investigators have reported similar data.

Experimental kinetic data indicate that we will not be able to use equilibrium compositions in making our modeling calculations.

We compare below the equilibrium composition of wet water gas at 900° C and 1000° C and the kinetic data of the reaction between the flowing gas (0.7 - 0.9 m/sec) and the carbon particles 2-3 mm. in the reactor (data according to [Kaftawov et al. (17)]).

| TEMPERATURE | EQUILIBRIUM COMPOSITION DATA | | COMPOSITION ACCORDING TO KINETIC DATA | | | |
|-------------------|------------------------------|-----------------|---------------------------------------|------|-----------------|------------------|
| | %CO | %H ₂ | %CO ₂ | %CO | %H ₂ | %CH ₄ |
| 900° C (1652° F) | 45 | 50 | 10.1 | 34.6 | 55.2 | 0.1 |
| 1000° C (1832° F) | 50 | 50 | 8.8 | 38.1 | 52.9 | 0.2 |

The equilibrium constant may be calculated from the Gibbs free energy (G): $\Delta G = R T \ln K$ where $\Delta G = \Delta H - T \Delta S$. The correlation between the equilibrium constant and the temperature is expressed usually by the equation ($p = \text{const}$):

$$\ln k = \frac{1}{R} \int \frac{\Delta H}{T^2} dT + a \text{ (where } a \text{ is an integration constant).}$$

Several difficulties are encountered in a discussion of the kinetics of coal gasification. Since the effects of coal devolatilization on the product gas rates are important up to temperatures between 600-700° C, usually only the data above 700°C are analyzed to obtain the kinetic constant. Laboratory experiments show that during the coal burn-off versus time studies a gradual induction period is followed by a region in which burn-off increased with a time. Instantaneous reactivity (R) may be calculated from the equation:

$$R_t = \left(\frac{1}{W_E} \right) \left(\frac{dw}{dt} \right)$$

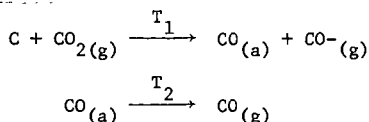
where W_E is the weight of the unreacted char on a dry-ash free basis and $\frac{dw}{dt}$ is the slope of the burn-off versus time. For the reaction in the air R_t increases and often W_E is replaced by W_0 (starting weight) and $\frac{dw}{dt}$ is taken for the maximum rate of weight loss.

The first principal reaction which occurs during the underground coal gasification process is the pyrolysis. The rate of pyrolysis as well as the amount and composition of the volatile products from a given sample of coal or char depends on the rate of heating, the final decomposition temperature, the vapor residence time and the environmental conditions such as applied pressure, particle size, coal type, etc. under which the pyrolysis takes place.

Normally pyrolysis starts at about 350°-400° C and is completed at about 1000° C. The reactivity with steam, oxygen, hydrogen or carbon dioxide during the pyrolysis of coal is mainly a function of the volatile matter and the rate of heating.

GASIFICATION RATE OF CHAR IN THE CARBON DIOXIDE ATMOSPHERE

The reaction between the char and carbon dioxide is hardly detectable below the temperature 800-900° C. According to Wen, C. Y. et al. (4) the activation energy is about 59.26 kcal/mole which indicates chemical-reaction control. The following mechanism was proposed by Walker (28):



Experimental data indicated that the order of reaction with respect to CO_2 can be assumed to be unity up to about one atmosphere pressure. However, at higher temperatures, the diffusion resistance within the solid particle may become significant and therefore an effectiveness factor must be introduced for such cases.

According to Wen et al. (4) the rate of the char-carbon dioxide reaction is found to depend on the coal origin more than on the gasification scheme used. The various rate characteristics of coals and chars are apparently due to the difference in their pore characteristics.

GASIFICATION RATE OF CHAR ON OXYGEN-ATMOSPHERE

The reaction rate in the temperature range 424-576° C using air was determined recently by C. Y. Wen et al. (4). The rate of reaction showed a maximum at a conversion of 10-50 percent; the maximum depended on the sample used. The observed

maximum reaction rate, dx/dt , was $1.67 \times 10^{-3} \text{ sec}^{-1}$. Under these conditions the reactivity of the char is determined by chemical kinetics and depends more on the extent of the gasification of the char rather than on the parent coal.

In the temperature range 834-1106° C, the reaction rates appear to correspond to a film-diffusion control regime. The rates do not change significantly with conversion degree until about 80 percent conversion is reached. Assuming a spherical particle shape, the average rate at 1000° C was $1.8 \times 10^{-6} \text{ g/cm}^2 \text{ s atm}$. A nitrogen-air mixture was used as the low oxygen concentration source.

THE GASIFICATION RATE OF CHAR IN THE HYDROGEN-ATMOSPHERE

A. Tomite et al. (26) investigated the reactivity of a char which was prepared at 1000° C. Usually the reactivity profile of a majority of the chars shows some slow induction period followed by a rate increase. The reaction rate generally increases as the rank of the parent coal decreases. Removal of mineral matter profoundly affects the reactivity profile of chars. In most cases the reaction rate decreases with mineral-matter removal.

The pseudo-activation energy changes from 150 kcal/mole to about 213 kcal/mole with increased conversion of the char.

According to Feistel et al. (6) the kinetic constant of hydrogasification is strongly affected by the hydrogen pressure and was expressed by the equation:

$$K_{H_2} = \frac{0.00402 \exp. (-5200/T) P^2_{H_2}}{1 + 0.000648 \exp. (4100/T) P_{H_2}}$$

The gasification rate with steam-hydrogen, resulted in the experimental equation, which shows a significant effect of the temperature upon the gasification rate.

The activation energy for the kinetic equation rate was 33,600 cal/ mole and the frequency factor was $2.51 \times 10^4 \text{ l/min}$.

THE REACTION RATE OF CHAR IN STEAM ATMOSPHERE

Linares et al. (19) found that in general the char reactivity was related to the steam reaction and decreased with an increase in the rank of the parent coal. However, a considerable spread in reactivities of char produced from coals of similar rank was observed. Removal of mineral matter diminished the char reactivity but the removal of mineral matter also resulted in a profound change in the surface area and porosity. The influence of each of these variables is difficult to access. Below 890° C the reaction is chemically controlled with an apparent activation energy of 42 kcal/mole. Above 890° C, the reaction is diffusion controlled and has an activation energy of 18 kcal/mole. The reaction rate was found to be proportional to steam pressure raised to the 0.60 power.

The rate of gasification of bituminous coal in the ($H_2O - H_2$) mixture in the temperature range 700-1100° C was investigated by Feistel et al. (6). The kinetic constant for steam decomposition was a function of steam pressure and temperature. The rate of reaction for a pressure higher than 10 atm. was described as:

$$\frac{dx_B}{dt} = K (1-x_B)$$

where x_B is base carbon conversion degree; t-time; k-kinetic constant

$$k_{H_2O} = \frac{1.88 \times 10^6 \exp(-2.24 \times 10^4/T) P_{H_2O}}{(1 + 1.56 \times 10^5 \exp(-1.65 \times 10^4/T) P_{H_2O}}$$

$$x_B = \frac{\text{base carbon gasified}}{\text{base carbon in feed coal char}} \quad (\text{according to Johnson})$$

THE CHAR REACTIONS IN THE CONDITIONS OF UNDERGROUND GASIFICATION

One possible approach is to calculate the residence time of the char in the high temperature zone of 1500-1800° F. The thickness of the coke zone (coal with 10 percent seam moisture) would be about 0.5 m; for the brown coal at 50 percent moisture this is about 15 cm assuming the advance rate of burning zone about 0.1×10^{-3} m/sec. The obtained residence time (40-130 hour range) implies that the seam moisture and volatile content are more significant factors than that of char reactivity upon the overall reaction rate.

THE EFFECT OF THE BLAST INTENSITY AND GASIFICATION ZONE ADVANCEMENT RATE ON THE HEATING VALUE OF PRODUCED GAS

A Russian investigation [Ludin *et al.* (20)] has shown that the optimum blast rate depends on the thickness of the coal seams. It was explained that the thicker seams have a larger water intrusion rate than the thinner seams. If air is used as the blast; there is an optimum water to air ratio that gives a maximum heating value of produced gas. On the other hand, it was observed the gasification front advancement increased with the higher blast rate. Therefore a certain gasification front advancement rate will correspond to the optimum gas heating value.

THE EFFECT OF THE PEAK GASIFICATION TEMPERATURE UPON THE HEATING VALUE OF THE GAS PRODUCED

The lower concentration of hydrogen caused by the lower temperature gasification does not necessarily lead to a low Btu product gas since a higher methane yield may be obtained in some cases. For example, Gregg *et al.* (10) found, during some underground tests, 6.3 percent of methane in the gas produced. Fisher *et al.* (7) made the observation that the presence of steam resulted in a higher concentration of methane in the produced gas. It could be explained that either the steam promotes the reaction of hydrogen and char or the following methanation reaction $CO + 3H_2 \rightleftharpoons CH_4$ occurs. This methanation reaction could be catalyzed by the mineral matter in the char.

INSTABILITY AND UNCERTAINTY FACTORS IN THE UNDERGROUND GASIFICATION MODELING

The following factors would lead to instability of the gasification process and may result in a large modeling error:

1. Change in coal and strata permeability.
2. Rapid water influx. The water may intrude upstream and go through the combustion zone or it may intrude downstream of the combustion zone. In theory an optimum water intrusion exists for any air blast injection. In practice of the gasification usually has a higher water intrusion rate than desirable and operates on the water rich side of optimum.
3. Rapid channeling of gasification process.
4. Rapid gas or air leakage to the strata.

The purpose of this study is to formulate a specific theoretical description of the forward combustion process of thin coal seams (one to several meters thick-

ness) and to establish the base which would allow to compare the model prediction to the eventual results of the field tests. It seems to be worthwhile to mention a few recent publications relating to the in situ gasification modeling. Different methods of gasification and various geological formation lead to different mathematical models. For example modeling were presented by Kotowski (18) and by Gunn and Whitman (12) in the study of reverse and forward combustion. Thorsnes described the evaluation of thermal front measurements and pressure drop versus flow rate. The longwall generator modeling was reported by Sawyer and Shuck (22). Some preliminary analysis was given by Gidaspow (9). The practical purpose of underground gasification modeling is to be able to predict the gas composition and permit the development of improved gasification control strategies. The experimental data [Yauagimoto (29)] have shown a significant effect of the gasification zone temperature upon the gas composition. It seems to be difficult to perform an adequate heat balance and to calculate the resulting temperature of the gasification zone considering such phenomena as: thermoplastic behavior as the coal is heated through a certain temperature; porous coke structure, contact area between the flowing gas and gassified coal etc. Therefore the measurements of the gasification zone temperature of the thin seams has been proposed. The equilibrium data calculated for the system volatile - gases from carbon reacting with oxygen, carbon dioxide etc. at the determined temperature, superimposed by the gas composition resulting from the kinetic of char burn out and shift reaction would give the resulting composition of produced gas.

MODELING OF GAS COMPOSITION FOR THE IN SITU GASIFICATION

The logical objectives of fitting equations to experimental data are twofold: to estimate the effect for each of the independent variables and to be able to predict the responses. The preliminary examination of experimental data should lead to:

1. Ordering (in the space or time)
 - a. List and magnitude of independent variables
 - b. Locate the clusters for estimation of error
2. Plotting
 - a. Factor or variable space
 - b. Time sequences

The next stage is the construction of specific equations according to the experimental data.

The calculation of gas composition requires a listing of independent experimental variables, as below:

1. Rate of air blast (and the oxygen concentration in the case of air enrichment). This factor is interrelated to the rate of gas production; temperature profile and flame front velocity.
2. Total rate of water moisture supply consisting of coal moisture; blast air moisture and water influx. This is obtained from the total mass balance and measurements.
3. Composition and rate of gas production.
4. Rate of carbon combustion (calculated from point 3.)
5. Coal properties such as moisture, ash, content of volatile, caloric value, conductivity.

6. Coal combustion characterization such as char reactivity, rate of pyrolysis reaction.
7. Temperature profile of the gasification zone with velocity flame front. The temperature profile follows from the total energy balance. Yanagimoto *et al.* (29) observed that the calorific value of the gas produced is sensitive to the combustion temperature of underground gasification.

The calculation program is presented below:

- 100 Mass balance of oxygen and total water. Water influx and air leakage (from material balance). Estimated cluster of errors.
- 200 The reaction rate and resulting gas composition at the equivalent average temperature of the gasification zone.
- 201 Pyrolysis of coal and the tar and gas composition derivated from Kinetic equations.
- 202 Rapid reaction (oxygen, hydrogen, steam) with volatile carbon. Gas composition derivated from equilibrium data.
- 203 Char reaction with gas phase (oxygen, carbon dioxide, steam). Gas composition derivated from kinetic data. The conversion reaction.
- 204 Calculation the resulting carbon monoxide, hydrogen and carbon dioxide concentration.
- 300 Energy balance and the temperature profile.
- 301 The general energy balance of the solid phase.
- 302 Heat sink by conduction for surrounding materials.
- 303 Heat sink by convection to the flowing gases.
- 304 Heat losses to the ash.
- 305 Heat used for the water-steam system.
- 306 Dependent factor: rate of combustion.
- 307 Problems related to the boundary conditions.

100 The conservation of mass equations for oxygen and total water would be as follows:

$$[\text{Rate of oxygen (water) mass in}]_1 - [\text{Rate of oxygen (Water) mass out}]_2 + [\text{Rate of generation of oxygen (water mass)}]_3 - [\text{Rate of accumulation of oxygen (water mass)}]_4 = 0$$

Due considerations have to be given for the moisture content of the air; the gasified coal; soil or rock; the strata of the roof in the area of gasified coal; and gravity influx of water respectively as well as the moisture dissociated in the heterogeneous reaction zone and the undissociated moisture in the heterogeneous reaction zone). The formula to calculate these water types has been summarized by Kalashinikov *et al.* (16). The mass balance of water (being in a form of coal moisture; the water influx and blast moisture) and its discrepancy would show the magnitude of seam water influx and the rate of steam decomposition rate. The continuity equation for these mass balances could be presented as follows:

$$\frac{\partial}{\partial X} (\Delta \text{ mass}) + \phi_m \cdot r + \frac{\partial}{\partial \text{time}} (\phi_m \cdot \Delta \text{ mass}) = \text{const.}$$

where Δm can be calculated as the weight fraction of the component in the injected air and $\phi_m \cdot r$ is an oxygen (water) reaction rate function. The mass balance of

oxygen and its discrepancy would indicate the gas (air) leakage rate and the rate of steam decomposition due to the reactions, e.g.,



200 The kinetic data concerning the coal devolatilization (pyrolysis) and the combustion of the matter devolatilized from coal should be applied if reliable prediction is to be obtained.

201 The kinetic rate (r) of coal pyrolysis under non-isothermal conditions can be described by two functions:

$r = \frac{d\alpha}{dt} = K(T) \phi(\alpha)$ where $a = \frac{Vt}{V_\infty}$, Vt is the volume of the product in time t and V_∞ is the final product volume attained at the end of the reaction. The function $K(T)$ is only temperature dependent, while $\phi(\alpha)$ is a function of the instantaneous phase composition. Using the Arrhenius equation one may obtain the final equation in which the rate of gas production is expressed as follows:

$$\frac{dv}{dt} = \frac{Av^\infty}{c} \exp \left[\frac{-E}{RT} - \frac{A}{C} \frac{RT^2}{E} e^{-E/RT} \right]$$

The heating rate is denoted here as $c = \frac{dT}{dt}$. As an example we use the following experimentally determined kinetic parameters (according to Campbell (2) for subbituminous coal types).

| GAS | PEAK AREA % | KINETIC PARAMETERS | |
|-----------------|-------------|------------------------|----------------------------|
| | | A (min ⁻¹) | E ^b (Kcal/mole) |
| H ₂ | 100 | 1.2 x 10 ³ | 22.3 |
| CH ₄ | 32.3 | 1.0 x 10 ⁷ | 31.0 |
| CO ₂ | 53.6 | 3.3 x 10 ⁴ | 19.5 |
| CO | 30 | 3.3 x 10 ³ | 18.0 |

Pyrolysis of the larger coal particles was described by Forrester (8).

202 The devolatilized compounds, resulting from the coal pyrolysis, burn with oxygen. The reaction rate of volatile compound is very high in the range of 0.5-2 sec. depending on the temperature of the gasification zone. Therefore, the assumption that the equilibrium composition is formed in this zone, seems to be justified. When the state of the system is such that $\Delta G = 0$ no process will occur and the system is at equilibrium. For a system consisting of n -species $\Delta G = \sum N_i \Delta g_i$ where N_i is the number of moles of i and Δg_i is the molar specific Gibbs function for species i .

If the Gibbs function has the minimum value then for any complete set of independent reaction

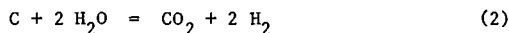
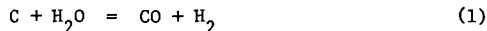
$$\frac{\partial \Delta G}{\partial \epsilon_i} = \sum_{j=1}^n \frac{\partial \Delta G}{\partial N_j} \frac{\partial N_j}{\partial \epsilon_i} = \sum_{j=1}^n (\beta_{ij} - \alpha_{ij}) \frac{\partial \Delta G}{\partial N_j} = 0$$

A procedure described in the literature as the Newton or Newton-Raphson method may be applied in order to solve the equations and to obtain numerical values. The computer calculations for the equilibrium data were described in the report of Combustion Engineering, Inc. (21).

203 The reaction of coal-char with the gases. The rate constant for the char reactions can generally be written in the Arrhenius form: $K = A \exp(E/RT)$ where E is the activation energy and the parameter A is the frequency factor and does depend on the number of molecules covering unit surface area. These values vary depending on the type of reaction and the carbon sample; for example, for the carbon-oxygen reaction it is from 20-80 Kcal/mole, for the carbon-steam reaction it is from 55-83 Kcal/mole [Isley *et al.* (14)] and for the carbon-carbon dioxide reaction it is from 26-84 Kcal/mole. Johnson (15) reported the kinetics of bituminous coal char gasification with gases containing steam and hydrogen.

The petrographic type and coal rank affects the char reactivity during gasification [Davis *et al.* (1)] so that the velocity constant for the coal type subjected to underground gasification should be determined experimentally. The manual of coal conversion fundamentals recently prepared by the Institute of Gas Technology presents a calculation procedure (using a char of a known reactivity factor) for the produced gas composition from a fluidized bed gasifier. However, for an average flame front velocity of about 0.1 cm per hr. in the underground gasification and for the resulting long residence time of char in a high temperature gasification zone, (30-130 hours) the char reactivity does not play a significant role.

The reaction of coal with steam and the resulting gas composition is defined by the kinetic of the two primary and two secondary reactions:



By denoting Z_i as the participation coefficient of the i reaction in the mixture, we would obtain [according to B. M. Derman (3)]:

$$Z_i = \frac{d(C_x) V_i}{\sum d(C_x)} \quad \text{and (e.g.)} \quad \frac{dc_1}{dc_{111}} = \frac{2 Z_3 + Z_1 - Z_4}{Z_1 + 2 Z_2 + Z_1}$$

Experimental data [Ludin *et al.* (26)] show that the conversion reaction occurs downstream from gasification zone is catalyzed by the inorganic matter in the coal. Therefore, the modification of the gas composition due to this reaction should be included in the last stage of a computation.

204 A hybrid computer program was prepared by NASA (TMx-3403) that can solve chemical kinetic systems with many chemical species for either a flow or static reactor.

300 Energy balance and temperature profile calculation approach.

301 The general solid phase (coal-char) energy balance may be presented as follows:

[Thermochemical heat from reactions] + [heat input (output) by conduction] - [convective loss to flowing gas] + [Extended loss e.g. ash] = [Net heat accumulated in solid phase].

Analysing the mass balance, the change in an accumulation of solid phase may be obtained from the equation:

[Carbon used by oxygen] + [Carbon used by carbon dioxide] + [Carbon used by the reaction with steam] = - [Change of solid accumulation].

The primary combustion reaction rate is controlled by the oxygen supply. One dimensional peak temperature and temperature profile are a function of the following parameters: the total heat generated by carbon combustion reactions, the total heat losses and dissipated energy resulted by the coal conductivity, water heating and evaporation, convective heat transfer from solid to flowing gases, and heat losses in the leftover ash. The endothermic reactions, e.g., between the steam and char, are usually considered as a portion of the carbon combustion reactions. The approximated results may be obtained using the calorific value of coal instead of the heat reaction.

In the one dimensional energy balance the total heat of the various reactions would be expressed:

$$\sum_{i=1}^n \Delta H_i \frac{\partial x_i}{\partial \text{time}} \mu = \text{total heat} \quad (1)$$

where x_i is stoichiometric coefficient of reaction and μ is a function of the solid phase which reacts with oxygen (carbon dioxide; steam).

320 We can now combine the heat transfer sink by conduction (solid) and the heat reaction representing uniformly distributed heat source and express it by the equation:

$$\frac{\partial}{\partial x} \left(K \frac{\partial t}{\partial x} \right) + \frac{\partial}{\partial y} \left(K \frac{\partial t}{\partial y} \right) + \frac{\partial}{\partial z} \left(K \frac{\partial t}{\partial z} \right) + \sum_{i=1}^{i=n} \Delta H_i \frac{\partial x_i}{\partial \text{time}} \mu = \rho c \frac{\partial t}{\partial \text{time}} \quad (2)$$

(t = temperature) This equation can be easily converted to the form containing the property $\left(\frac{k}{\rho c}\right) = \alpha$ which is the thermal diffusivity coefficient. Several authors (American and Russian) have confirmed that the temperature peak of coal combustion depends on this coefficient. However, the porous-capillary property of coal-char material requires further modification of the equation due to the convective transport associated with forced air and the gas flowing through the body. This should include the coolant mass flow (G_c) and the porosity of the material $\left(\frac{G_c}{K_e}\right)$. For one dimensional conduction equation (2) becomes:

$$\frac{\partial^2 t}{\partial x^2} + \frac{G_c \cdot C_c}{K_e} \frac{dt}{dx} + \frac{\sum \Delta H_i \frac{\partial x_i}{\partial t} \mu}{K} = \frac{1}{\alpha} \frac{\partial t}{\partial \text{time}} \quad (3)$$

Depending on the boundary conditions various types of solution of this type of equation may be obtained. If we assume that the high temperature gasification zone may be represented as a porous plate cooled on our side, then the general solution of the equation (3) becomes:

$$\frac{t - t_x}{t_a - t_x} = \frac{Bi}{Bi + F} e^{-p (\alpha/s)} \quad (4)$$

where Bi is the Biot number and F is a Fourier number.

303 Further steps should include the heat losses by convection from the solid to the flowing gases. The significant portion of this type of heat loss is related to heating of the nitrogen and the water vapors.

The heat transfer from solid surfaces to the flowing gases and water vapor can be conveniently expressed in terms of a nondimensional Nusselt number, $Nu = \frac{hD}{K}$, where

h is the heat transfer coefficient, K is the thermal conductivity of the gas and D is a characteristic dimension. For turbulent flow, $Nu = f(Re)$ where Re is a Reynolds number.

A significant difference of opinion exists as to whether or not a turbulent flow type occurs during the gasification in situ [Hahn & Debrand (13)]. It probably depends on the local circumstances of gasification such as cracks size, channeling, surface area of the channels, etc. Therefore a practical solution would include an estimation of this loss by the equation:

$$\frac{Q \text{ convective}}{V \text{ nitrogen}} = h (T \text{ average} - T \text{ inlet}) \quad (5)$$

where V nitrogen is the flow rate of nitrogen in the blast air; T inlet gas temperature, T average - temperature of gasification zone.

304 A significant effect of the ash content upon the peak temperature of gasification zone was observed experimentally. Some experimental data has shown that the exothermic reaction of ash formation does not compensate for the latent heat of the ash left in the gasification zone. The estimated heat losses would be proportional to the ash content in the coal and the rate of the coal combustion ($\frac{\Delta m}{\text{time}}$):

$$Q_{\text{ash}} = K_1 \cdot \Delta \text{ Ash content} \cdot \frac{\Delta m \text{ carbon}}{\text{time}} \quad (6)$$

305 Based on the water heat balance, the heat use for the water evaporation and the water vapor latent heat, should be included. This heat would be proportional to the moisture content of the coal and the rate of the coal combustion:

$$Q_{\text{water}} = K_2 \Delta \text{ water content} \frac{\Delta m \text{ carbon}}{\text{time}}$$

306 The width and the rate of advancement of the gasification zone are proportional to the rate of the blast air. The coal combustion rate is also controlled by the supply of oxygen and in this context, the oxygen supply rate is the only independent factor.

~~In the circumstances in which the water supply (influx) can be controlled, the ratio of total moisture/oxygen supply effects the following parameters:~~

- a) The equilibrium and the kinetics of the combustion reaction as well as changes in the balance of the thermochemical heat of the gasification reaction.
- b) The change of the temperature in the gasification zones due to the endothermic reaction of steam decomposition and the heat sink is determined by the heat related to the water evaporation, latent heat of steam and heat losses to the strata.

The total solid phase energy balance would include the above mentioned inter-related expressions for the nonsteady heat transfer and the definition of the boundary conditions. The limitation of these calculations lie in the assumed boundary conditions. Further study is needed in this area.

REFERENCES

1. Davis Alan, William Spackman; Peter Given, Energy Sources, page 55, Vol. 3 No. 1 (1976).
2. Cambell, J. H., Lawrence Livermore Laboratory, Report No. UCRL-52035, March 1976.

3. Derman, B. M. Academia Nauk CCCP, Trudy Institute Gorutchih Iskopaemyh XIII, page 19 (in Russian).
4. Dutta, S., Wen, C. Y., Ind. Eng. Chem. Proc. Des. Dev., Vol. 16, No. 1 p. 20 and p. 31, 1977.
5. Daniel Cuthberg and Fred Wood; Fitting Equations to Data, Wiley-Interscience, Inc., New York, 1971.
6. Feistel, P. P., Van Hook, R. R. Juntgen, 173rd ACS Meeting March 21-25, 1977, Vol. 22, No. 1, page 53.
7. Fischer, J., et al., Argonne National Laboratory, Report No. ANL-77-7, December, 1976.
8. Forrester, III, R. C., ERA, Vol. 1, No. 4, pos. 4501, Conf., 750870-1.
9. Gidaspow, D., Paper No. 4D, Presented at the 83rd ASCE National Meeting, Houston, Texas, March, 1977.
10. Gregg, D. W., Hill, R. W., Olness, D. U., Lawrence Livermore Laboratory, Report No. UCRL-52004, January, 1976.
11. Gregg, D. W., Olness, D. U., ERDA Report No. UCRL - 52107, August, 1976.
12. Gunn, R. D., and Whitman, D. L., Laremie Energy Research Center, Report No. L ERC/RI-76/2, Feb., 1976.
13. Hahn, O. J., and Debrand, S., Heat Transfer Limitation for Underground Gasification of Thin Coal Seams., Paper presented at the 83rd National Meeting of the American Institute of Chemical Engineers, Houston, Texas, March 20, 1977.
14. Ilsley, J. M., et al., Principles of Gasification Reactions Department of Fuel Tech. University of Sheffield, Page 1.
15. Johnson, J. L., Coal Gasification ACS Advances in Chemistry Series No. 131 p. 145-78 (1974).
16. Kaleshnikov, P. J. et al., UCRI, Trans. 10899. Tr. Vsesoy, Nauch, Inst. Ispol. Gas. No. 2, p. 97, 1967.
17. Kaftanov, S. V., Fedosev: Khimia Tverdogo Topliva, Vol. 10, No. 4, p. 83, 1976.
18. Kotowski, M. D., and Gunn, R. D., ERDA Report No. LERC-RI/76/4, March, 1976.
19. Linares, A., Mahajan, O., Walker, P. L., 1973rd Meeting ACS, March 21-25, 1977, Vol. 22, No. 1, p. 1.
20. Ludin, J. D., Krugov, O. W., Makerova, M. J., and Birukov, W. F., Laboratory of the Coal Gasification, Page 19 (in Russian).
21. Mathematical Modeling of Chem. Processes for Low Btu Gasification Combustion Engineering Inc., Windsor, Conn., August, 1976.
22. Sawyer, W. K., Shuck, L. Z., Society of Petr. Eng. of ASME, Paper No. SPE 5743.
23. Schora, F. C., Sixth Synthetic Pipeline Gas Symposium, Chicago, Ill, October, 1974, page 27.
24. Stewart, T. and Wall, T. E., Sixteenth International Symposium on Combustion (1977)
25. Stephens, D. R., and Miller, D. G., Lawrence Livermore Laboratory, Report No. UCJD-17245, August, 1976.
26. Tomite, A. et al. 1973rd ASC Meeting, March 21-25, 1977, Vol. 22, No. 1, p. 4, Fuel Vol. 56, p. 137, 1977.
27. Thorsness, C. B., Lawrence Livermore Laboratory, Report No. UCID-17007, Jan. 19, 1976.
28. Walker, P. L. et al., 173rd ACS Meeting March 21-25, 1977, Vol. 22, No. 1, Page 7
29. Yanagimoto, et al., ERDA Energy Research Abstracts, ERA, Vol. 1, No. 8, pos. 12397.
30. Yang, R. et al., 173rd ACS Meeting, March 21-25, 1977, Vol. 22, No. 1, p. 19.

METALLURGICAL COKES FROM OXIDIZED HIGHLY CAKING COALS

B. Ignasiak, D. Carson, P. Jadernik, and N. Berkowitz

Alberta Research Council, Fuel Sciences Division
Edmonton, Alberta, Canada T6G 2C2

ABSTRACT

Laboratory studies suggest that improvements of coke strength brought about by preheating caking coals before carbonization accrue from inadvertent oxidation rather than from physical changes in the coal mass due to removal of moisture. Controlled oxidation of highly caking coal, followed by carbonization, produces cokes which, in terms of strength, are equivalent to those obtained from prime metallurgical blends. Appropriately formulated blends of exhaustively oxidized and fresh caking coal similarly yield cokes whose properties are comparable to those cokes made from the same coal after oxidation under optimum conditions.

In exercising quality control over the manufacture of metallurgical cokes, it is frequently found useful to preheat the oven-charge in an inert atmosphere at some temperature between 150° and 350°C. The principal benefit of such treatment is a substantially shortened carbonization cycle (1,2) and, hence, greater oven productivity; but in some instances, it has also been observed to result in somewhat greater strength of the finished cokes, and this has been attributed to higher bulk density and better thermal conductivity of the charge after removal of moisture (2).

Bearing in mind that even very slight oxidation affects the rheological properties of caking coals (3), and that preheating tends to reduce their maximum dilatation (4), it appears, however, just as likely that greater coke strength accrues from inadvertent oxidation of the coal during preheating, and the study reported below does, in fact, indicate this to be the more correct view.

EXPERIMENTAL

For the purposes of this investigation, three Appalachian hvAb coals (see Table 1), all characterized by high (Gieseler) fluidity and very pronounced (maximum) dilatation (see Table 2), were used.

In one set of experiments, samples of these coals were preheated for varying periods of time in a sand bath at $180 \pm 3^\circ\text{C}$ while commercial "pure" nitrogen or helium (from Canadian Liquid Air Ltd. and Union Carbide Canada Ltd., respectively) was passed through them at $\sim 10 \text{ ml min}^{-1}$. In a second, the same procedure was used, but the inert gas was thoroughly purified by passing it through a fixed bed of metallic nickel on lamp black at 800°C (5) before admitting it to the coal samples.

After cooling to room temperature in the protective atmosphere, portions of the preheated samples were then tested for their dilatometric and fluidity characteristics, and others were carbonized as previously described (6) and submitted to coke strength tests. Strength was expressed in terms of the F_{5-45} Index (6) which, over a wide range of values, is directly proportional to the ASTM coke stability factor.

To avoid a basis for comparison with oxidized coal, one of the test coals (No. 3) was also exposed to oxygen (at 200°C) and to air (at 100°C and 150°C) for varying periods of time, and then examined like the preheated samples.

RESULTS AND DISCUSSION

After preheating under thoroughly purified nitrogen or helium for 24 hours, the rheological properties of all three coals were found to be entirely unchanged. But preheating under commercial "pure" nitrogen or helium caused rapid loss of fluidity and progressive decrease of the (maximum) dilatation - although at the same time very significantly raising the strength of the coke obtainable from the preheated coal. Figure 1, in which the bracketed numbers refer to coke strength, illustrate these effects for preheating in nitrogen. (Preheating in helium yielded very similar results, except that fluidities then decreased even faster, possibly due to a higher residual oxygen content of this gas.)

The enhanced coke strengths shown in Figure 1 are qualitatively paralleled by the variation of the strengths of cokes made from variously oxidized coal No. 3 (see Figure 2). As anticipated, the oxidation period to optimum oxidation depended on the severity of the treatment, and thus ranged from 15 minutes (for oxygen at 200°C) to 60 hours (for air at 100°C). But in all three cases, a limited oxidation of the coal before carbonization is seen to result in quite dramatic improvements of coke quality. The total oxygen contents of the coal samples after optimum pre-oxidation and oxidation to total loss of caking properties are shown in Table 3.

Verification of the conclusion that slight "accidental" oxidation of the coal during preheating increases coke strength was obtained from semi-technical-scale tests in a 500 lb movable wall oven*. In one test, fresh No. 3 coal was charged, and in a second, preheated No. 3 (96 hours at 170-190°C) was carbonized. Preheating was done in an externally gas-heated hopper through which commercial "pure" nitrogen was passed at 900 ml min⁻¹ (see Figure 3).

The data obtained from evaluation of the two coke lots made in the experimental oven are shown in Table 4 and established a 10 point improvement in the ASTM stability factor when the preheated charge was used. But perhaps even more interesting, in the control of this study, is the variability of coke strengths observed when smaller (20 lb) samples, withdrawn from different locations in the hopper, were carbonized in the laboratory. This variation is graphically presented in Figure 4 in which the bracketed numbers at the sampling points show the maximum dilatation of the preheated coal before carbonization. Comparison of Figures 3 and 4 shows that the point of nitrogen entry into the hopper charge - which is presumably also the point at which the highest concentration of contaminant oxygen would be encountered - lies in a zone from which maximum coke strengths and minimum dilatation were recorded.

Since Figure 4 shows the preheated hopper charge to have been almost as heterogeneous as a coal blend, one further series of laboratory carbonization experiments was carried out with variously formulated blends of fresh and "exhaustively" oxidized coal No. 3. ("Exhaustive" oxidation here means oxidation to total loss of caking properties.) The results of these tests are summarized in Figure 5 and show that, irrespective of the manner of oxidation, addition of oxidized coal can be an effective means for maximizing coke strength. Scanning electron micrographs (see Figure 6) underscore this conclusion by showing that the microscopic structure of cokes made from optimally composed blends of fresh and exhaustively oxidized coal No. 3 compares very favorably with that of coke made from a prime mvb caking coal alone.

*These tests were conducted in collaboration with the Energy Research Laboratories, Department of Energy, Mines and Resources, Ottawa. Fuller details of this program will be published elsewhere.

ACKNOWLEDGEMENTS

We are indebted to Professor T. H. Patching, Department of Mineral Engineering, University of Alberta, for the micrographs, and to Mr. J. C. Botham and his staff for assistance in conducting tests in the movable-wall coke oven.

REFERENCES

1. Beck, K. B., 25th Canadian Conference on Coal, Victoria, B.C., Sept. 16-19, 1973.
Jackman, H. W. and Helfinstine, R. J., Illinois State Geological Survey, Circular 423, 1968; Circular 434, 1968; Circular 449, 1970, Circular 453, 1970.
Dukham, V. N. and Gryaznov, N. S., Koks Khim., 1967, (7) 6.
Yoshida, S. and Sato, H., Nenryo Kyokaishi, 1966, 45 (472), 563.
Yoshida, Y., Nenryo Kyokaishi, 1966, 45 (476), 898.
Dietrich, W., Engschuber, M., and Fritzsche, E., Energietechnik, 1969, L9 (4) 168.
Holub, Y., Sb. Pr. UVP, 1969 (13) 5.
2. Rohde, W. and Beck, K. G., Gluckauf, 1973, 103 (6) 1.
3. Ignasiak, B., Nandi, B. N., and Montgomery, D. S., Fuel (Lond.) 1970, 43, 214.
Ignasiak, B., Clugston, D. M., Montgomery, D. S., *ibid.*, 1972, 51, 76.
Ignasiak, B., Szladow, A. J., and Montgomery, D. S., *ibid.*, 1974, 53, 12.
Ignasiak, B., Szladow, A. J., and Berkowitz, N., *ibid.*, 1974, 53, 229.
4. Beck, K. G., personal communication.
5. Ignasiak, B., Nandi, B. N., and Montgomery, D. S., Analytical Chemistry, 1969, 41, 1676.
6. Ignasiak, B., and Berkowitz, N., Bull. Canada Inst. Min. Metall., 1974, 67, No. 747, 72.
Carson, D., Ignasiak, B., and Berkowitz, N., *ibid.*, 1976, 69, No. 766, 100.

Table 1. Composition of Test Coals

| Coal | Rank | Proximate analysis, % | | | | Fixed Carbon (d.a.f.) | Calorific Value (Gross) BTU/lb. | Ultimate analysis, % (d.a.f.) | | | |
|------|------|-----------------------|-----------------|---------------|------|-----------------------|---------------------------------|-------------------------------|-----|-----|-----|
| | | (Capacity) Moisture | Ash (dry basis) | V.M. (d.a.f.) | | | | C | H | N | S |
| 1 | hVAb | 2.1 | 4.2 | 32.3 | 67.7 | 14,510 | 87.6 | 5.4 | 1.6 | 0.8 | 4.6 |
| 2 | hVAb | 1.7 | 6.3 | 34.2 | 65.8 | 14,290 | 87.3 | 5.5 | 1.6 | 1.5 | 4.1 |
| 3 | hVAb | 2.0 | 5.3 | 36.9 | 63.1 | 14,270 | 86.0 | 5.5 | 0.9 | 0.7 | 6.9 |

* by difference

Table 2. Rheological Properties of Test Coals

| Coal | FSI | (Gieseler) plasticity | | | | Ruhr-dilatation | | | | |
|------|-----|-----------------------|-----------------------|------------------|-----------------------|-----------------|-----------------------|-----------------------|---------------|-----|
| | | Soft. temp., °C | Max. fluid. temp., °C | Solid. temp., °C | Max. fluid. temp., °C | Soft. temp., °C | Max. contr. temp., °C | Max. dilat. temp., °C | Max. dilat. % | |
| 1 | 8 | 403 | 455 | 491 | 3600 | 365 | 423 | 519 | 27 | 182 |
| 2 | 8 | 400 | 443 | 476 | 13100 | 355 | 401 | 611 | 23 | 394 |
| 3 | 8 | 400 | 443 | 475 | 8200 | 369 | 412 | 487 | 29 | 122 |

Table 3. Oxygen Contents of Oxidized No. 3 Coal.
(Initial [O] = 6.2%)

| Oxidation method | Oxygen contents, (% w/w) | |
|------------------|---------------------------|--|
| | after "Optimum" Oxidation | after Oxidation to Total Loss of Caking Properties |
| Air at 100°C | 6.7 (60)* | 7.4 (410) |
| Air at 150°C | 7.1 (6) | 7.8 (22) |
| Oxygen at 200°C | 6.4 (0.25) | 10.1 (0.75) |

* Bracketed numbers show time of oxidation (hrs) to oxygen contents.

Table 4. Evaluation of Cokes from Tests in 500 lb Movable-Wall Oven

| | ASTM Stability Factor, (%) | Factor, (%) | Breeze, (% of ½ in fraction) |
|---|----------------------------|-------------|------------------------------|
| 1. Fresh Coal | 35.2 | 64.5 | 3.9 |
| 2. Preheated Coal (Nitrogen; 170-190°C, 96 hrs) | 45.8 | 64.5 | 3.6 |

FIGURE 1. VARIATION OF MAXIMUM DILATATION (---) AND MAXIMUM (GIESELER) FLUIDITY (---) WITH DURATION OF PREHEATING IN COMMERCIAL "P URE" NITROGEN. (BRACKETED NUMBERS SHOW THE STRENGTH INDICES OF COKES.)

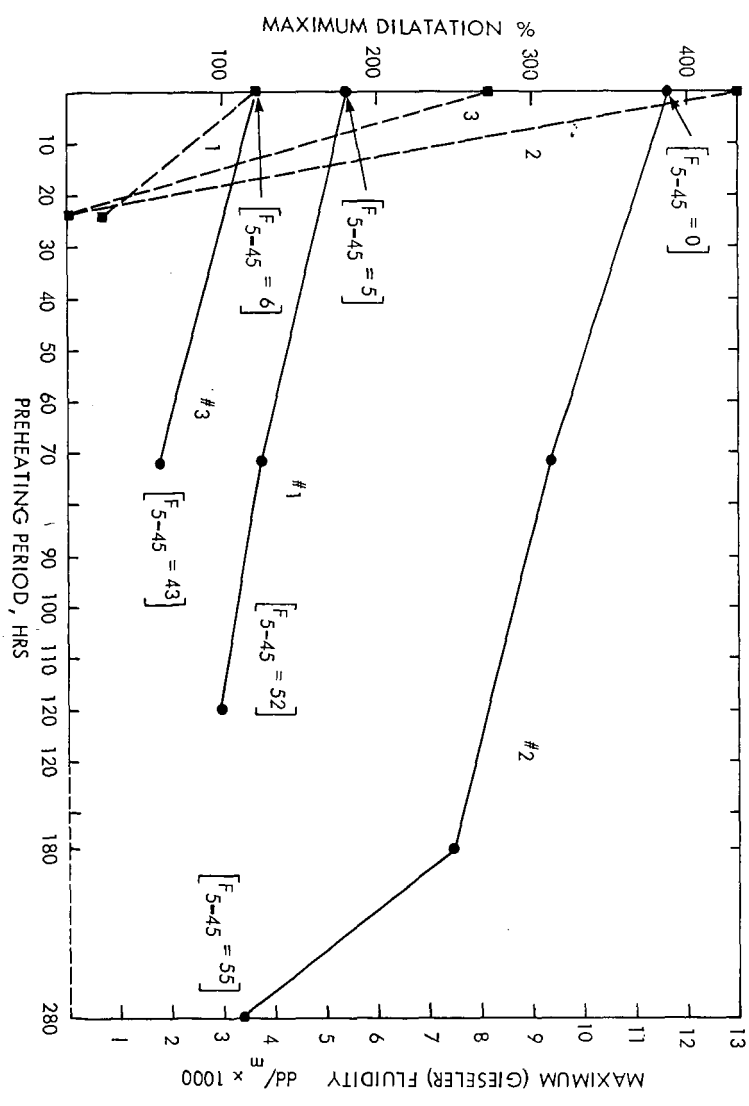


FIGURE 2. EFFECT OF OXIDATION ON STRENGTH OF COKES FROM COAL NO. 3

- A. OXYGEN AT 200°C
- B. AIR AT 150°C
- C. AIR AT 100°C

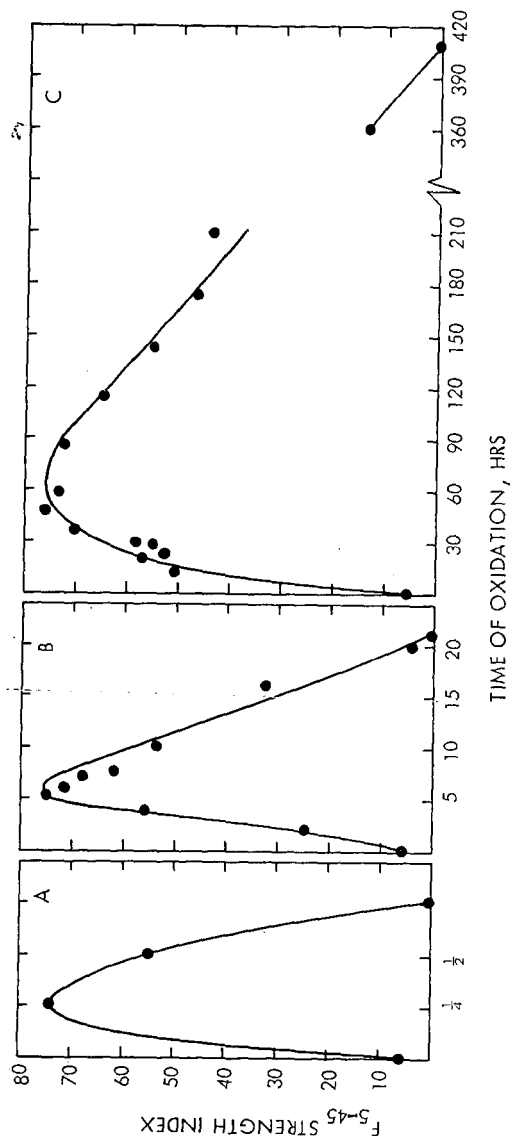


FIGURE 3. PREHEAT HOPPER FOR 500-LB

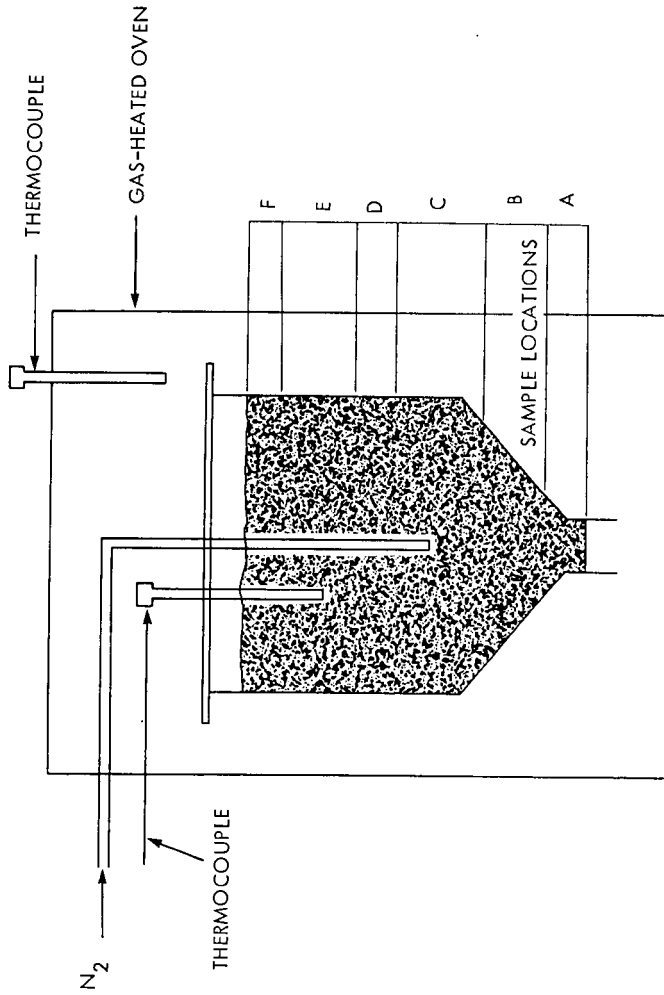


FIGURE 4. MAXIMUM DILATION OF PREHEATED NO. 3 COAL SAMPLES AND STRENGTH OF COKES AS FUNCTIONS OF LOCATION IN PREHEAT HOPPER.

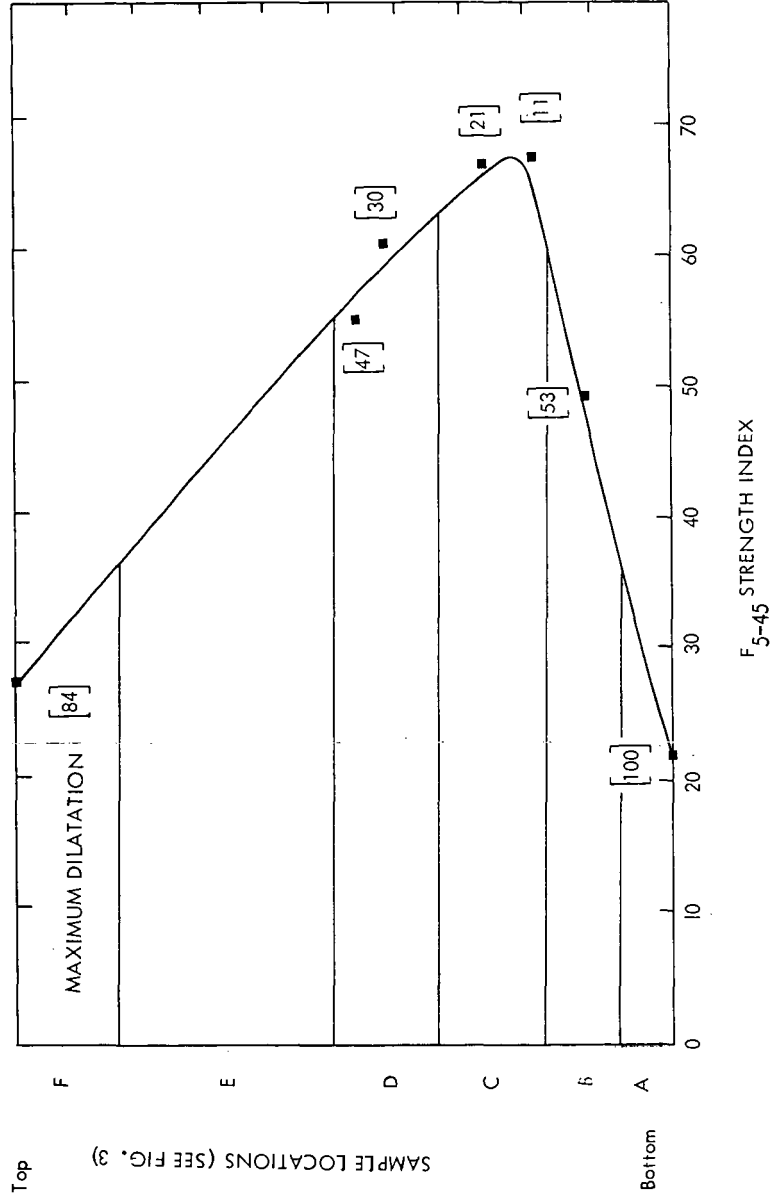
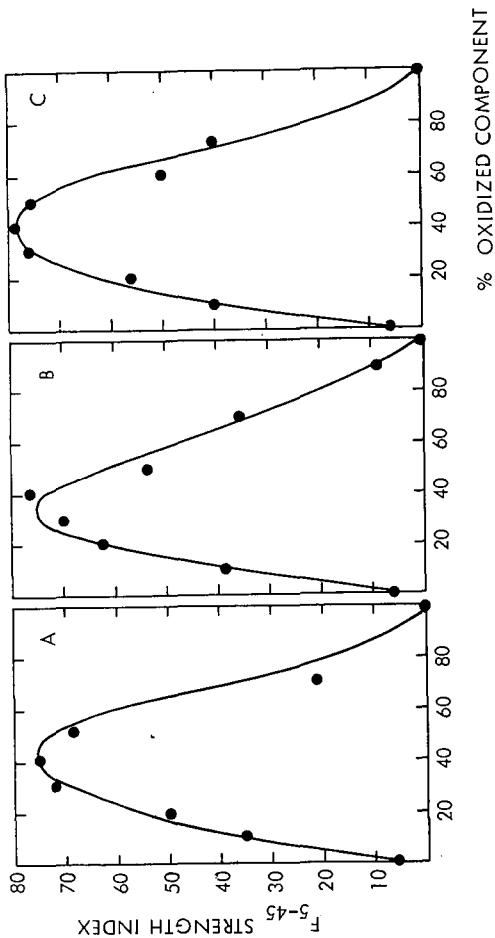
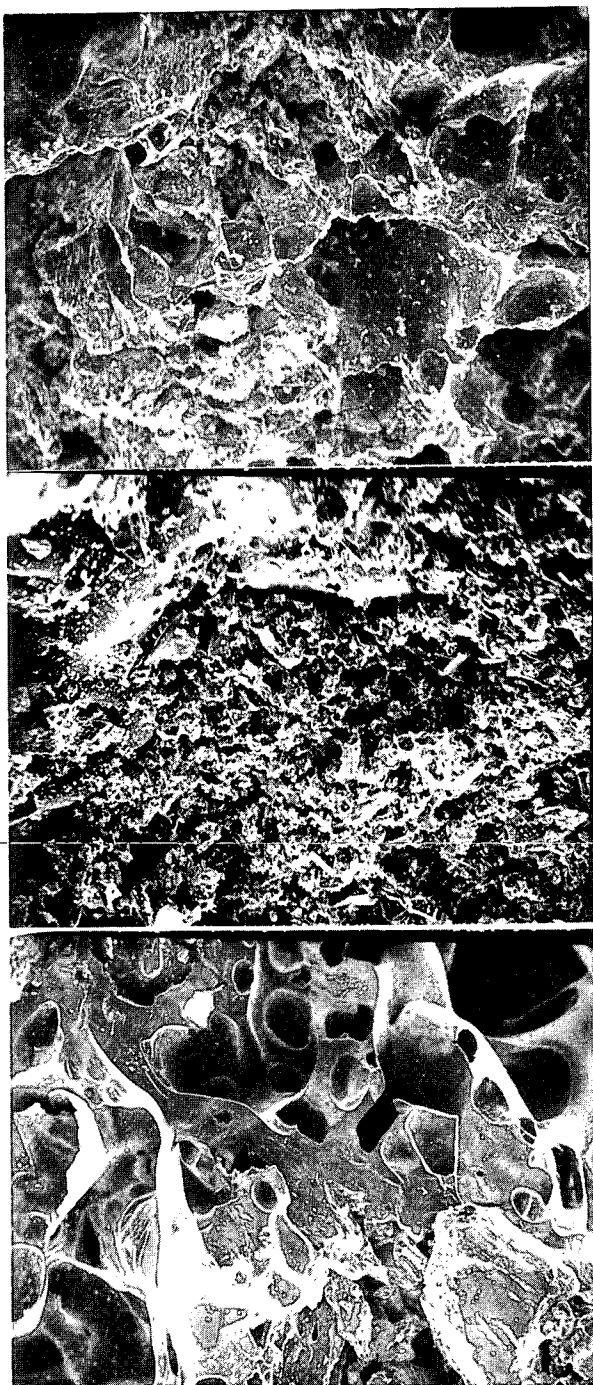


FIGURE 5. STRENGTH OF COKES FROM BLENDS OF FRESH AND "EXHAUSTIVELY"
 OXIDIZED COAL NO. 3.
 (OXIDIZED COMPONENT PREP. BY TREATMENT WITH)
 A. OXYGEN AT 200°C, 2.5 HRS
 B. AIR AT 150°C, 22 HRS
 C. AIR AT 100°C, 407 HRS





A.

B.

C.

Figure 7. Scanning Electron Micrographs ($\times 100$) of cokes

A. - coke from a blend containing fresh (60 parts) and "totally" oxidized (40 parts) No. 3 coal

B. - the same as A but in the 80:20 ratio

C. - coke from mvb prime coking coal from Cardinal River

MOSSBAUER SPECTROSCOPY OF IRON IN COAL AND COAL HYDROGENATION PRODUCTS

Bernard Keisch,^{1/} Gerst A. Gibbon^{2/} and Sayeed Akhtar^{2/}

^{1/} Carnegie-Mellon Institute of Research
4400 Fifth Avenue, Pittsburgh, PA 15213

^{2/} U. S. Department of Energy
Pittsburgh Energy Research Center
4800 Forbes Avenue, Pittsburgh, PA 15213

ABSTRACT

The chemical states of iron in a Kentucky coal and in the products of its hydrogenation were determined by Mössbauer spectroscopy. The iron in the coal was present chiefly as pyrite, FeS_2 . There was, however, evidence for some non-pyritic iron, most likely present as szomolnokite ($\text{FeSO}_4 \cdot \text{H}_2\text{O}$). The products from hydrogenation of this coal by the SYNTHOIL process⁴ at 723 K and 28 MPa contained all the iron as FeS_x where $x = 1.0$ to 1.14. There was no evidence for unreduced FeS_2 or FeSO_4 . There was also no evidence for elemental iron. At the experimental conditions for hydrogenation of coal in this work, the reactor gas contained 0.32 percent H_2S . Evidently, FeS_x is not reduced to elemental iron in the presence of this concentration of H_2S in the reducing gas.

INTRODUCTION

Iron is a major constituent of the mineral matter in many U. S. Coals (1). The metal occurs principally as iron pyrite, FeS_2 , in coal although small quantities of the element may be present as sulfate, oxide, carbonate or silicate (2, 3). In several Australian brown coals, significant quantities of iron occur as salts of carboxylic acids (4, 5, 6). An investigation of iron in coal by Mössbauer spectroscopy was first reported by Lefelhocz *et al.* (7). From an examination of seven U. S. coals ranging in rank from lignite to anthracite, they concluded that, in some coals, iron occurs exclusively as FeS_2 , and non-pyrite iron, when present, occurs as Fe(II) in a high-spin configuration.

The purpose of the present investigation was to determine, by Mössbauer spectroscopy, the iron compounds in a coal utilized in the SYNTHOIL process and in the process products. In this process, a feed paste consisting of pulverized coal in recycle oil is reacted with hydrogen at 723K (450°C) and 14-28 MPa (2000-4000 psi) in a turbulent-flow reactor packed with pellets of Co-Mo/SiO₂-Al₂O₃ catalyst. The product stream is cooled and the gross liquid product, after separation from gases, is centrifuged to remove the unreacted solids. The centrifuged liquid product is a low-sulfur, low-ash fuel oil a portion of which is used as recycle oil to prepare more feed paste for continuous process operation (8, 9).

"By acceptance of this article, the publisher and/or recipient acknowledges the U. S. Government's right to retain a nonexclusive, royalty-free license in and to any copyright covering this paper."

EXPERIMENTAL

Samples of feed coal, feed paste, gross liquid product, centrifuged liquid product and centrifuged residue were drawn from a 1/2 ton per day SYNTHOIL plant currently in operation at the Pittsburgh Energy Research Center. The basics of the plant and the sampling points are shown in figure 1. A detailed description of the procedure and precautions required for obtaining representative samples has been published by Schultz *et al.* (10). The origin and analysis of the coal are given in table 1. The hydrogenation was conducted at 723K and 28MPa.

Samples were placed in circular plastic containers, 25 mm in diameter and 3 mm deep, for Mössbauer analysis. The containers were covered with plastic discs and mounted horizontally in the spectrometer so that any settling of the solids from the liquid samples was uniform with respect to the gamma ray beam. The source was ^{57}Co diffused in Cr. The Mössbauer spectrometer used was of conventional design (Nuclear Science Instruments, Inc.*) and the spectra were obtained by transmission. Iron foil was used for velocity calibration and also provided the reference for isomer shifts. All spectra were recorded at room temperature ($\sim 300\text{K}$).

RESULT AND DISCUSSION

The weights of samples, the results of chemical analyses for iron in each of them and the spectrometer run times are given in table 2. Isomer shifts, quadrupole splittings, ΔS 's and approximate strengths of the internal magnetic fields are given in table 3. The literature values of the Mössbauer parameters for a number of pertinent iron compounds are presented in table 4.

The Mössbauer spectrum of the feed coal showed two strong peaks with an isomer shift of 0.32 mms^{-1} and a quadrupole splitting of 0.64 mms^{-1} . These values agree well with the isomer shift and quadrupole splitting values reported in literature for pyrite and marcasite, two naturally occurring minerals of composition FeS_2 (7, 13). The Mössbauer parameters for the two minerals are so similar that their spectra cannot be resolved if both are present. Although Mössbauer analysis is unable to distinguish pyrite from marcasite, petrographic and X-ray diffraction studies have shown that FeS_2 in coals is generally pyrite (20, 21). Specifically, the FeS_2 in the present coal has been shown by Ruch, *et al.* to be iron pyrite (22).

The spectrum of the coal also showed a single, very weak peak with a velocity of 2.83 mms^{-1} relative to the source. This, no doubt, corresponds to one peak of the doublet for non-pyrite iron reported by Lefelhocz *et al.* in several coals (7). They determined an isomer shift of about 1.1 mms^{-1} (recalculated with reference to iron) and a quadrupole splitting of about 2.6 mms^{-1} . Unfortunately, the second peak for non-pyrite iron in our spectrum is completely obscured by one of the strong pyrite peaks, probably that with a velocity of 0.22 mms^{-1} relative to the source. Lefelhocz *et al.* concluded that the non-pyrite iron may be organic iron or inorganic iron as a silicate (7). Montano (27), however, observing similar

*Use of brand name facilitates understanding and does not necessarily imply endorsement by the U. S. Department of Energy.

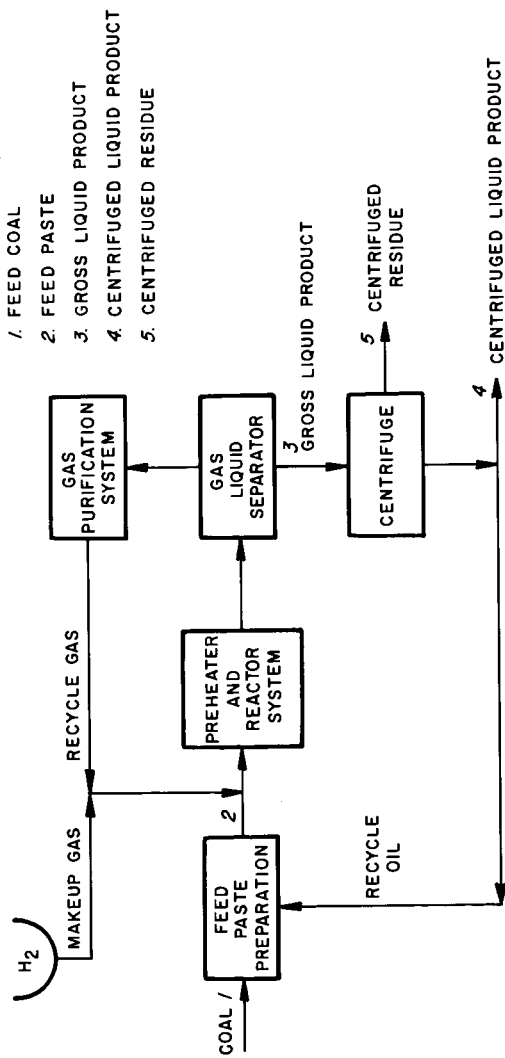


Figure 1 - Sampling points in the SYNTHOIL 1/2 ton per day unit

Table 1. - Analysis of the as-received feed coal¹

Proximate analysis, (wt. pct.)

| | |
|-----------------|------|
| Moisture | 6.1 |
| Volatile matter | 36.3 |
| Fixed carbon | 42.1 |
| Ash | 15.5 |

Ultimate analysis, (wt. pct.)

| | |
|---------------------------|------|
| Hydrogen | 4.9 |
| Carbon | 60.3 |
| Nitrogen | 1.2 |
| Oxygen (By difference) | 12.8 |
| Ash | 15.5 |
| Sulfur | 5.3 |
| as sulfate | 0.58 |
| as pyrite | 2.69 |
| as organic | 2.03 |

Rank: hvBb

¹A blend from Kentucky seams No. 9, 11, 12 and 13 which are mined together; Homestead mine, Western Kentucky. The coal was pulverized to a fineness of 70 percent through 200 mesh, U. S. Standard Sieve, and 100 percent through 100 mesh.

Table 2. - Samples analyzed by Mossbauer spectrometry

| Material | Weight (g) | Iron content (wt. pct.) | Spectrometer run time (hr.) |
|-------------------------------|------------|----------------------------|--------------------------------|
| Feed coal | 1.24 | 3.58 | 113 |
| Feed paste | 2.60 | 1.47 | 160 |
| Gross liquid product | 2.40 | 1.84 | 139 |
| Centrifuged liquid product | 2.16 | 0.55 | 189 |
| Centrifuged residue | 3.20 | 10.1 | ~100 |

Table 3. Results of Mössbauer Analysis

| Material | Isomer shift ^{1/} (mms ⁻¹) | Quadrupole splitting (mms ⁻¹) | ΔS^2 / (mms ⁻¹) | Approximate interval magnetic field ^{2/} H_I , (kOe) |
|------------------------------------|--|--|--|---|
| Feed coal | 0.32 ^{4/} | 0.64 | -- | -- |
| Feed paste | 0.32 ^{5/} | 0.63 | -- | -- |
| Gross liquid product ^{6/} | 0.59 | -- | 0.55 | 280 |
| Centrifuged liquid product | 0.70, 0.74 | -- | 0.00, 0.15 | 310, 270 |
| Centrifuged residue ^{6/} | 0.72 | -- | 0.28 | 280 |
| | 0.69, 0.72 | -- | 0.05, 0.69 | 310, 270 |

^{1/} Relative to iron

^{2/} Calculated from the 4 outer peaks of a 6-peak pattern as follows: $\Delta S = (S_6 - S_5) - (S_2 - S_1)$.

^{3/} $H_I = (S_6 - S_1) * 31$ where S_1 and S_6 are the outermost peaks of a six-peak pattern.

^{4/} An additional low intensity (5%) peak was observed at a velocity of 2.83 mms⁻¹ with respect to the source; see text for discussion.

^{5/} Calculated from the predominant doublet of the 6-peak spectrum.

^{6/} Discussion of multiple values given in text.

Table 4. Literature Values of Mössbauer Parameters for Some Pertinent Fe Compounds.

| Compound | Isomer shift δ (mms ⁻¹) | Quadrupole splitting (mms ⁻¹) | ΔS (mms ⁻¹) | Internal Magnetic field H_i (kOe) | Reference ^{2/} |
|--|---|--|------------------------------------|---|-------------------------|
| FeS (troilite) | 0.77 | 0.28 | | 310 | (11) |
| FeS _{1.14} (pyrrhotite) | 0.64 | | 0.16 | 307 | (11) |
| | 0.69 | | 0.31 | 225 | |
| FeS _{1.00} | 0.71 | | -0.32 | 308 | (12) |
| FeS _{1.05} | 0.82 | | -0.40 | 276 | (12) |
| FeS _{1.07} | 0.77 | | -0.52 | 275 | (12) |
| FeS ₂ (pyrite) | 0.28 | 0.60 | | | (7) |
| | 0.29 | 0.61 | | | (13) |
| FeS ₂ (marcasite) | 0.25 | 0.50 | | | (7) |
| | 0.23 | 0.51 | | | (13) |
| FeSO ₄ ·H ₂ O (szomolnokite) | 1.2 | 2.62 | | | (26) |
| Fe (metal) | 0.00 | | 0.00 | 330 | (14) |
| αFe ₂ O ₃ | 0.43 | 0.17 | | 515 | (17) |
| Fe ₃ O ₄ | 0.30 | | | 492 | (16) |
| | 0.63 | | | 455 | |
| FeO | 1.08 | 0.55 | | | (18) |
| αFeOOH | 0.35 | | 0.6 | 384 | (15) |
| FeSO ₄ | 1.25 | 2.94 | | | (17) |
| FeSO ₄ ·4H ₂ O | 1.32 | 3.17 | | | (18) |
| FeSO ₄ ·7H ₂ O | 1.31 | 3.20 | | | (18) |
| Fe ₂ (SO ₄) ₃ × H ₂ O | 0.45 | 0.28 | | | (19) |
| FeCO ₃ | 1.25 | 1.80 | | | (16) |
| Fe(HCO ₂) ₂ (formate) | | 1.86 | | | (16) |

Table 4. Literature Values of Mössbauer Parameters for Some Pertinent Fe Compounds (Continued).

| Compound | Isomer shift ^{1/} δ (mms) | Quadrupole splitting (mms ⁻¹) | ΔS_{-1} (mms ⁻¹) | Internal Magnetic field H_i (kO _e) | Reference ^{2/} |
|--|--|--|---|--|-------------------------|
| Fe(C ₂ H ₃ O ₂) ₂ (acetate) | 0.42 | 0.50 | | | (14) |
| Fe ₂ (CO) ₉ | 0.08 | 0.37 | | | (17) |
| Fe ₃ (CO) ₁₂ (-85°C) | 0.10 0.15 | 1.09 | | | (19) |

^{1/} Relative to iron. The following correction values were used: Stainless steel to iron -0.90 mms⁻¹, sodium nitroprusside to iron -0.26 mms⁻¹.

^{2/} The numbers refer to the bibliography at the end of the text.

spectra concluded that the non-pyrite fraction is anhydrous iron (II) sulfate FeSO_4 . But the literature values (28) he quotes for isomer shift and quadrupole splitting are inaccurate, as the experiment was probably inadvertently performed on $\text{FeSO}_4 \cdot \text{H}_2\text{O}$. More recent work, using carefully prepared materials, gave values for FeSO_4 and $\text{FeSO}_4 \cdot \text{H}_2\text{O}$ as shown in table 4. Assuming that, in our spectrum, the hidden peak of the high spin doublet is directly under the low velocity peak of the pyrite spectrum our values for the isomer shift and quadrupole splitting would be $\sim 1.3 \text{ mms}^{-1}$ and $\sim 2.6 \text{ mms}^{-1}$, respectively, which are in excellent agreement with $\text{FeSO}_4 \cdot \text{H}_2\text{O}$ as are Montana's and Lefelhocz's.

The spectrum of the feed paste was a composite of the spectra of its components, namely the feed coal and the recycle oil. The latter, as explained above, is a portion of the centrifuged liquid product from a previous batch. For convenience, therefore, the spectrum of the feed paste will be discussed after discussing the spectrum of the centrifuged liquid product.

The spectra of the gross liquid product, the centrifuged liquid product and the centrifuged residue were similar and may be discussed together. Each of the spectra showed a six-peak pattern with isomer shifts in the range of 0.69 to 0.74 mms^{-1} , ΔS 's in the range of 0.00 to 0.69 mms^{-1} and the strengths of the internal magnetic fields in the range of 310 to 270 kOe. The outermost peaks in the spectra of the gross liquid product and the centrifuged residue showed partial resolution into two subpeaks. The values of the isomer shifts, the ΔS 's and the strengths of the internal magnetic fields given in table 3 for these two materials are the values obtained by using the positions of the outer and inner subpeaks respectively to calculate the parameters. Hafner and Klavins observed similar fine structures in the Mössbauer spectra of two pyrrhotites and used a comparable technique for data reduction (11). A comparison of the Mössbauer parameters in tables 3 and 4 shows that the gross liquid product, the centrifuged liquid product and the centrifuged residue contain Fe_x where $x = 1.0$ to 1.14.

In agreement with our findings, Ruch et al. found pyrrhotite in the centrifuged residue by X-ray diffraction analysis of aliquots drawn from the samples used in this work (22).

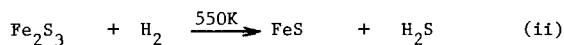
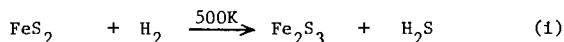
The spectrum of the feed paste had six peaks: two strong peaks corresponding to the pyrite peaks in the spectrum of the feed coal, and four weak peaks, two on each side of the strong doublet. The four weak peaks correspond to the outer four peaks in the size-peak spectrum of the centrifuged liquid product. The two middle peaks of the centrifuged liquid product are obscured by the two strong peaks of the pyrite. Clearly the spectrum of the feed paste is a composite of the spectra of coal and centrifuged liquid product, the components of the feed paste.

None of the spectra obtained in this work showed any absorptions other than those discussed above. We estimate the precision of our measurements is such that other compounds (for example, those shown in table 4 starting with iron) would have been detected had they been present in significant

amounts. Elemental iron, Fe_2O_3 , Fe_3O_4 , or $\alpha\text{-FeOOH}$ would have been detectable in any of the materials analyzed if present in quantities as small as 5% of the total iron present. In the case of the feed coal, the detection limits for iron and above oxides would have been even lower and, in addition, the presence of many of the other compounds in the lower portion of Table 4 would have also been detectable at the 5% level. Possible exceptions are the iron (III) sulfates, iron (III) acetate and $\text{Fe}_2(\text{CO})_9$ with detectability limits of the order of 10-20%.

Although the feed coal does contain a small amount of $\text{FeSO}_4 \cdot \text{H}_2\text{O}$, the quantity of it is too small to account for all the sulfate the coal is known to contain by conventional analysis (see Table 1). Some of the sulfate is presumably combined with Ca or some other cation.

The spectra of the gross liquid product, the centrifuged liquid product and the centrifuged residue showed no evidence for elemental iron. The absence of iron is significant since Gallo has reported the reduction of FeS_2 to elemental iron by the following successive reactions (23):



These results were obtained with gavorranto, a natural pyrite, containing 97.12 percent FeS_2 . It should be noted that reaction (iii) is reversible and, therefore, the reduction of FeS to Fe will not be feasible if the partial pressure of H_2S in the reducing gas is above some critical value. Rosenquist has measured K_p for reaction (iii) at 723K (24). At 28 MPa hydrogen pressure, the equilibrium H_2S pressure is 0.008 percent of the hydrogen pressure. In the present study, the reactor gas contained approximately 0.32 percent H_2S and, evidently, FeS_2 was not reduced to iron in the presence of this concentration of H_2S .

In the qualitative agreement with our results, J. T. Richardson has reported that FeS_2 is reduced to Fe_7S_8 ($\text{FeS}_{1.14}$) during coal hydrogenation (25). By thermomagnetic analysis of a char from a coal liquefaction plant he concluded that the iron in char was present as a mixture of Fe_7S_8 and FeS_2 . The exact composition of the mixture varied with the process conditions.

CONCLUSIONS

Mössbauer analysis of a Kentucky coal showed that iron in the coal was present mainly as FeS_2 . There was some non-pyritic iron, most likely present as szomolnokite ($\text{FeSO}_4 \cdot \text{H}_2\text{O}$). Products from hydrogenation of the coal at 723K and 28 MPa contained FeS_x where $x = 1.0$ to 1.14. There was no evidence of elemental iron in the products.

ACKNOWLEDGEMENTS

We thank Andrew G. Sharkey, Jr., Robert A. Friedel and Paul M. Yavorsky of Pittsburgh Energy Research Center for their interest in this work. A. G. Sharkey, Jr. and R. A. Friedel also participated in several technical discussions.

REFERENCES

1. Abernethy, R. F., Peterson, M. J., and Gibson, F. H., 1969. Major Ash Constituents in U. S. Coals, USBM/RI-7240. U. S. Bureau of Mines, Pittsburgh, PA, pp. 4-9.
2. Thiessen, G., 1945. Composition and Origin of Mineral Matter in Coal. In: H. H. Lowry (Editor), Chemistry of Coal Utilization John Wiley & Sons, New York, p. 487.
3. Dutcher, R. R., White, E. W., and Spackman, W., 1964. Elemental Ash Distribution in Coal Components - Use of Electron Probe. In: Proceedings of the 22nd Ironmaking Conference, Iron and Steel Division, Metallurgical Society of A.I.M.M.E., pp. 463-483.
4. Shaffer, H. N. S., 1977. Organically Bound Iron in Brown Coal. Fuel, 56:45.
5. Brooks, J. D., Durie, R. A. and Sternhell, S., 1958. Chemistry of Brown Coal II. Infrared Spectroscopic Studies. Australian Journal of Applied Science, 9:63.
6. Brooks, J. D. and Sternhell, S., 1957. Brown Coals I. Oxygen-Containing Functional Groups in Victorian Brown coals. Australian Journal of Applied Science, 8:206.
7. Leflhocz, J. F., Friedel, R. A., and Kohman, T. P., 1967. Mössbauer Spectroscopy of Iron in Coal. Geochimica et Cosmochimica. Acta, 31:2261.
8. Akhtar, S., Mazzocco, N. J., Weintraub, M., and Yavorsky, P. M., 1975. SYNTHOIL Process for Converting Coal to Nonpolluting Fuel Oil. Energy Communications, 1:21.
9. Yavorsky, P. M., Akhtar, S., Lacey, J. J., Weintraub, M., and Reznik, A. A., 1975. The SYNTHOIL Process. Chemical Engineering Progress, 71:79.
10. Schultz, H., Gibbon, G. A., Hattman, E. H., Booker, H. B., and Adkins, J. W., 1977. The Distribution of Some Trace Elements in the 1/2 Ton Per Day SYNTHOIL Process Development Unit. PERC/RI-77/2. Pittsburgh Energy Research Center, Pittsburgh, PA, pp. 2-6.
11. Hafner, S. and Klavius, M., 1966. The Mössbauer Resonance of Fe⁵⁷ in Troilite (FeS) and Pyrrhotite (Fe_{0.88}S). Zeitschrift für Kristallographie, 123:443.
12. Ono, K., Ito, A., and Hirahara, E., Mössbauer Study of Hyperfine Field, Quadrupole Interactions and Isomeric Shift of Fe⁵⁷ in FeS_{1.00}, FeS_{1.05} and FeS_{1.07}. Journal of the Physical Society of Japan, 17:1615.
13. Temperley, A. A. and Leferve, H. W., 1966. The Mössbauer Effect in Marcasite-Structure Iron Compounds. Journal of the Physical Chemistry of Solids, 27:85.

14. Muir, A. H., Ando, K. J., and Coogan, H. M., 1966. Mössbauer Effect Data Index, Interscience, New York, 351 pp.
15. Forsyth, J. B., Hedley, I. G., and Johnsen, C. E., 1968. The Magnetic Structure and Hyperfine Field of Graphite (αFeOOH). Journal of Physics C (Proceedings of the Physical Society, Ser. 2, 1:179).
16. Stevens, J. G. and Stevens, V. E., 1972. Mössbauer Data Index (covering 1971 literature), Plenum, New York, 430 pp.
17. Stevens, J. G. and Stevens, V. E., 1972. Mössbauer Data Index (covering 1970 literature), Plenum, New York, 369 pp.
18. Stevens, J. G. and Stevens, V. E., 1970. Mössbauer Data Index (covering 1969 literature), Plenum, New York, 281 pp.
19. Fluck, E., Kerler, W., and Neuwirth, W., 1963. The Mössbauer Effect and Its Application for Chemistry. *Angewandte Chemie*, 75:461. (In German).
20. Thiessen, G., Ball, C. G., and Grohs, P. E., 1936. Coal Ash and Coal Mineral Matter. *Industrial and Engineering Chemistry*, 28:355.
21. Mitra, B. G., 1954. Identification of Inorganic Impurities in Coal by the X-Ray Diffraction Method. *Fuel*, 33:316.
22. Ruch, R. R., Gluskoter, H. J., Dreher, G. B., Russel, S. J., Cahill, R. A., Frost, J. K., Kuhn, J. K., Steele, J. D., Thomas, J. and Malhotra, R., 1977. Determination of Valuable Metals in Liquefaction Process Residues. Quarterly Technical Progress Report No. 18 to U. S. ERDA, under contract (E46-1)-8004 20 pp.
23. Gallo, G., 1927. The Reduction of Iron Ores With Hydrogen. *Annalen Chemie Applicata*. 17:39. (Chemical Abstracts, 1927, 21:1243²).
24. Rosenquist, T., A Thermodynamic Study of the Iron, Cobalt, and Nickel Sulphides., *Journal of the Iron and Steel Institute*, 176:37.
25. Richardson, J. T., 1972. Thermomagnetic Studies of Iron Compounds in Coal Char. *Fuel*, 51:150.
26. Gallagher, P. K., Johnson, D. W. and Schrey, F., 1970. Thermal Decomposition of Iron (II) Sulfates. *Journal of the American Ceramic Society*, 53:660.
27. Montano, P. A., 1977. Mössbauer Spectroscopy of Iron Compounds in West Virginia Coals. *Fuel*, 56:397.
28. Grant, R. W., Widersick, H., Muir, A. H., Gonser, U. and Delgass, W. N., 1966. Sign of the Nuclear Quadrupole Coupling Constant in Some Ionic Ferrous Compounds. *Journal of Chemical Physics*, 45:1015.

An Infrared Absorption Study of Coal-Metal Salt Catalyst Interactions

J. M. Lee*, R. E. Wood and W. H. Wiser, Mining and Fuels Engineering Department, University of Utah, Salt Lake City, Utah 84112. *Present address, Department of Chemical Engineering, Auburn University, Auburn Alabama.

Introduction

A thorough study of the infrared absorption patterns produced by coal samples conducted by Friedel, et. al., (1) resulted in the assignment of absorption bands to specific structures or components of coal. Those assignments of importance to this study are listed in Table I.

Although some uncertainty exists with respect to these assignments the 3030 cm^{-1} band is considered to represent the aromatic C-H and the 2920 cm^{-1} and 2850 cm^{-1} bands represent aliphatic C-H. CH_3 , CH_2 , and CH (aliphatic) configurations all contribute to these absorption bands but the dominant effect is that from CH_2 because of its relative abundance. However, the IR differentiation does not discriminate between aliphatic C-H bonds in aliphatic side chains, in hydroaromatic structures, in cycloparaffins or in aliphatic connecting bridges. The 1610 cm^{-1} band is assigned to double bond carbon and/or carbon only bonds. In coal this is taken to be aromatic carbon (2,3). The 1450 cm^{-1} band is assigned to aliphatic H bending and/or aromatic carbon stretching. The 1260 cm^{-1} band is assigned to phenoxy and ether structures. Figure 1 shows these band assignments as derived by Friedel (1) and applied to the IR pattern of a thin section of vitranite.

Temperature effects on functional groups in coal have been studied by several authors (1,3,4,5,6). These reports indicate that the IR band assigned to the OH structures in bituminous coals disappears near 500°C. The band attributable to phenoxy structures (1260 cm^{-1}) decreases in intensity at 300°C but does not completely disappear even at 550°C. The C-H stretching band intensities decrease and the aromatic C-C and C-O band (1610 cm^{-1}) is unchanged at temperatures approaching 600°C. Oelert (4) has published an extensive interpretation of thermally induced structural changes in coal as a result of IR measurements.

The present study is an attempt to use the IR absorption procedure to measure change in coal structure under nitrogen and hydrogen (one atmosphere pressure) and in the presence of metal salt catalysts.

Experimental

A Beckman IR-20 Infrared Spectrophotometer was used to measure infrared spectra of KBr pellets containing finely dispersed coal and char samples. Kapaiowitz, Utah coal sized to 44-53 microns (-270 +325 mesh) was used. Proximate and ultimate analyses of this coal are given in Table II.

Coal samples were impregnated with metal salt catalysts (ZnCl_2 , CdCl_2 , $\text{SnCl}_2 \cdot 2\text{H}_2\text{O}$, $\text{CoCl}_2 \cdot 6\text{H}_2\text{O}$ and $\text{FeSO}_4 \cdot 7\text{H}_2\text{O}$) by mixing the coal with a water

solution of the salt and drying the slurry under vacuum at 110°C. The catalyst application rate was 0.112 moles of catalyst per 100 grams of MAF coal. The prepared sample (50 mg) was heated to various temperatures (250, 350 or 450°C) for 30 minutes in the presence of either H₂ or N₂ gas (99.98 % purity). Figure 2 shows a schematic drawing of the equipment used for heat treatment.

Following reaction, the chars were weighed to permit a correction for loss of volatile matter and KBr pellets were prepared. Twenty mg of each sample were ground in a Wig-L-Bug vibrator for 1 hour. Then, 0.5 to 2.0 mg of the coal or char were mixed with 250 mg of IR grade KBr for 10 minutes in the same device. Two hundred mg of the mixture were briquetted in a hot die (110 C) after evacuation. The result was a clear pellet 13 mm in diameter and 0.6 mm thick. Each sample was measured 4 times, not as duplicates, but at 0.2, 0.4, 0.6, and 0.8 weight percent of the KBr disc.

Results and Discussion

Figure 3 shows the IR pattern to be expected from different amounts of coal dispersed through a KBr pellet. Because the grinding and mixing were done in polystyrene vials there is an obvious contamination of this polymer in the sample as measured by the spectrometer. In fact, because the polystyrene contains similar bonding to that found in coal, the spectra of KBr with no coal present (but with polystyrene contamination) is very similar to the pattern obtained when coal is present. The effect of this contamination becomes constant at 10 minutes grinding or mixing time and hence is a constant which can be subtracted from the KBr plus polystyrene plus coal pattern.

Beer's law for absorption states that:

$$A = km/S + A_0 = k M/100S + A_0 = Kc + A_0$$

where A = sample absorbance at a specific absorption band

A₀ = constant absorbance due to the polystyrene

k = specific extinction coefficient (cm²/mg)

m = weight of coal in the disc (mg)

S = area of disc (cm²)

M = weight of the disc (mg)

c = weight percent of coal in the disc

K = slope of the line A vs c

The values of k, K and A₀ as measured for this study are shown in Table III for the 2920 cm⁻¹ absorption peak. Some literature values of k are included for comparison. Because the data obtained using the conventional base line (3120-2780 cm⁻¹) did not yield a straight line of A vs c for either the 2920 or 3030 cm⁻¹ bands, a second base line (3740-2200 cm⁻¹) was used. This base line provided the desired straight line function and also gave larger values of k and K without significantly changing A₀. Slopes were calculated for each of the A vs c lines (K values in the Beer law relationship). Correlation coefficients (r²) were calculated for

all the lines and data points generated. Statistically, all data points gave r^2 values in excess of the 90 percent confidence level and most cases were in excess of the 95 percent level.

Subsequent calculations have included data for N_2 and H_2 atmosphere, 350 and 450°C and no catalyst, plus the metal salts listed above. The data obtained on samples treated at 250°C were not included because of overlap of lines caused by water absorption with lines used in the calculations. For statistical purposes, the data provide two levels of atmosphere, two levels of temperature and two levels of catalyst application for each of the 5 metal salts used. The total data (K values) accumulated are included in Table IV. Changes in K values from one condition to another indicate an increase or a decrease in the type of bonding that gives rise to that particular absorption band. Therefore, changes in K values can be related to changes in aromatic hydrogen, aliphatic hydrogen, aliphatic carbon, etc., in the coal or char structure.

The infrared absorbance data were analyzed by means of a multivariable linear regression analysis procedure to discover which absorbances were statistically related. The percent volatile matter from each trial was included as the dependent variable in the computation. The correlation coefficients shown in Table V are the result of this calculation. The following comments can be made with respect to these correlation values.

1. The 3030 cm^{-1} absorbance peak (aromatic hydrogen) has a negative correlation with all other peaks, but a positive correlation with volatile matter. Although the correlation is not high in any case it means that the concentration of aromatic bonding in the char increases with increase in volatile matter production. This supports the concept that aromatic bonds are produced in the char as more volatile matter is produced.

2. All the absorbance bands, except 3030 cm^{-1} , have a negative correlation with respect to volatile matter. This indicates that the bonds represented by the absorbance bands, aliphatic or naphthenic hydrogen, aromatic carbon, carbonyl, carboxylates, phenoxy structures, etc., are destroyed or removed to produce volatile material.

3. A very good correlation coefficient (+0.785) is found for the 2920 and 2850 cm^{-1} bands. This supports the concept that these two bands measure the same thing, in this case aliphatic or naphthenic hydrogen.

4. Good positive correlation coefficients between 1610, (aromatic C and/or C=O), 1450 (CH_2 , CH_3 , C-C) and 1260 (C=O in phenoxy structures) indicate that they are also a measure of the same thing, or at least that the bonds they measure are affected simultaneously by the various sample treatment procedures.

5. The fairly good inverse correlation between the 2920 and 2850 cm^{-1} absorbance bands and the percent volatile matter is in agreement with published ideas on the origin of volatile components. The changes found in aliphatic hydrogen bonding indicate a decrease with increased volatile matter. This can be explained as abstraction of hydrogen from hydroaromatic structures by thermally produced free radicals, a second order reaction, (8,9) or by a first order pyrolytic breaking of aliphatic bonds (10,11).

6. The positive, but low, correlation between 2920 and 2850 cm^{-1} with 1610, 1450 and 1260 cm^{-1} indicates that the bonds responsible for these

absorbances are again treated similarly by the various sample treatment procedures. Although the bonds involved may not be the same, the various peaks do increase or decrease together.

The significance of the numerical (K) data of Table V was tested with the conventional F ratio, using three variables, each at two levels. The results of this study are shown in Table VI. In this table, the significance is noted by a number which is the statistical probability of error. The number 0.20 indicates a 1 in 5 probability that the statement is in error, 0.05 indicates a 1 in 20 probability that the statement is in error, 0.01 indicates a 1 in 100 and 0.001 indicates a probability of 1 in 1000 that the statement is in error.

Analysis of Table VI tells us that little difference is realized by virtue of hydrogen pressure at one atmosphere. FeSO_4 affects both the 3030 and the 2850 cm^{-1} absorption bands when hydrogen is present. Since both are increased, the Ar/Al ratio as represented by 3030/2920 is not affected. ZnCl_2 depresses volatile matter evolution at low temperature but increases it at high temperatures when hydrogen is present. CdCl_2 does act to increase volatile matter evolution when hydrogen is present. The 1610 cm^{-1} band is not affected by hydrogen presence with any of the metal salts.

Temperature acts to increase volatile matter evolution with all of the salts present. However, this volatile matter is obtained at the expense of different bonds in the presence of different salts. SnCl_2 and CdCl_2 act to increase aromatic hydrogen while FeSO_4 acts to decrease the aliphatic hydrogen at higher temperatures. CdCl_2 is the only salt of the five tested which does not decrease the aromatic carbon at the higher temperature.

The catalytic effect, as opposed to hydrogen or temperature, is shown in the final section of Table VI. ZnCl_2 acts to decrease the absolute amount of aromatic hydrogen in the char while SnCl_2 acts to cause an increase. This would appear to be an anomaly but can be explained if we assume that these salts influence different bonds. ZnCl_2 may influence hydrogen release from aromatic structures with consequent polymerization of the residual groups. SnCl_2 may influence hydrogen abstraction from hydroaromatic structures yielding aromatic structures in the residue which are less condensed than with ZnCl_2 . ZnCl_2 increases the aliphatic hydrogen as does FeSO_4 . For ZnCl_2 this indicates a transfer of hydrogen from some aromatic to form some aliphatic structures. ZnCl_2 , CdCl_2 and CoCl_2 decrease the ratio of aromatic hydrogen to aliphatic hydrogen while SnCl_2 increases it. SnCl_2 , CdCl_2 and FeSO_4 decrease the absolute content of aromatic carbon. SnCl_2 acts to increase volatile matter evolution while FeSO_4 has a slight tendency to repress the evolution. Other salts seem to have no effect on the final quantity of volatile matter evolved.

As a summary we can say that infrared absorption technique is capable of differentiating some types of bonds affected by coal pyrolysis in the presence of metal salts. Further, these salts do not act uniformly with respect to specific bonds. This is especially apparent in the cases of ZnCl_2 and SnCl_2 , both of which are effective as coal hydro-generation-liquefaction catalysts. ZnCl_2 acts to decrease the absolute content of aromatic hydrogen bonding while SnCl_2 acts to increase the absolute quantity of aromatic hydrogen in the char.

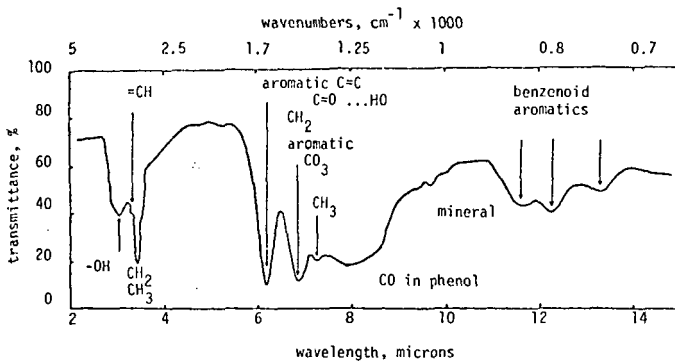


Figure 1. Infrared Spectrum of Vitrain Thin Section

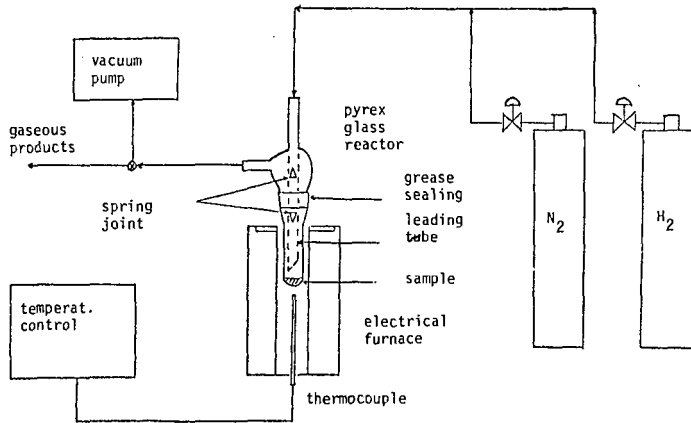


Figure 2. Flow Scheme of Reactions with N_2 and H_2

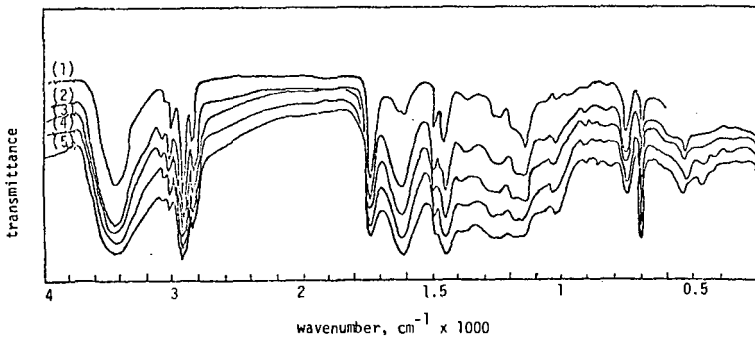


Figure 3. Spectra by Varying the Hiawatha Coal Concentration in the KBr Pellet; (1) KBr alone, (2) 0.218%, (3) 0.420%, (4) 0.600%, (5) 0.807%

TABLE I
Selected Infrared Absorption
Absorption Assignments in the Coal Structure (1)

| Absorption Band, cm^{-1} | Assignment |
|-----------------------------------|---|
| 2920 | Naphthenic and/or aliphatic C-H |
| 3030 | Unsaturated CH, probably aromatic |
| 1610 | Aromatic C-C and/or C-O...HO-; carboxilates |
| 2850 | Naphthenic and/or aliphatic C-H |
| 1450 | CH_2 and CH_3 ; aromatic C-C or ionic carbonates |
| 1260 | C=O in phenoxy structures |

TABLE II
Proximate and Ultimate Analysis
of Kaiparowitz, Utah Coal

| Dry Basis | | MAF Basis | | | | |
|-----------|--------|-----------|------|------|------|-------|
| % Ash | % V.M. | % C | % H | % N | % S | % O |
| 10.8 | 51.4 | 73.4 | 6.17 | 1.91 | 0.55 | 18.00 |

TABLE III
Constants Obtained From Beer's Law, 2920 cm^{-1}

| Coal Sample | k | K | A_0 |
|---|--------------|-------|-------|
| This work 3120-2780 base | 0.27 | 0.401 | 0.245 |
| 3740-2200 base | 0.40 | 0.599 | 0.264 |
| Freidel (1) 3120-2780 base vitrain (84% C) | 0.17 | | |
| Fujii (7) 3210-2780 base vitrain (83.4% C) vitrain (84% C) | 0.38 0.42 | | |

TABLE IV
K Values Obtained from IR Spectra

| A | T | C | 3030 | 2850 | 2920 | 1610 | 1450 | 1260 | V.M.% |
|----------------|-----|-------------------|-------|-------|-------|-------|-------|-------|-------|
| N ₂ | 350 | None | 0.184 | 0.263 | 0.268 | 0.835 | 0.636 | 0.547 | 6.9 |
| N ₂ | 450 | " | 0.214 | 0.234 | 0.207 | 0.751 | 0.611 | 0.537 | 21.8 |
| H ₂ | 350 | " | 0.223 | 0.307 | 0.388 | 0.787 | 0.648 | 0.474 | 6.2 |
| H ₂ | 450 | " | 0.258 | 0.267 | 0.247 | 0.789 | 0.711 | 0.497 | 24.7 |
| N ₂ | 350 | ZnCl ₂ | 0.200 | 0.245 | 0.382 | 0.819 | 0.587 | 0.478 | 7.1 |
| N ₂ | 450 | " ² | 0.159 | 0.367 | 0.426 | 0.654 | 0.524 | 0.523 | 21.4 |
| H ₂ | 350 | " | 0.155 | 0.335 | 0.466 | 0.819 | 0.675 | 0.548 | 6.4 |
| H ₂ | 450 | " | 0.171 | 0.286 | 0.401 | 0.789 | 0.692 | 0.512 | 25.4 |
| N ₂ | 350 | SnCl ₂ | 0.227 | 0.341 | 0.404 | 0.734 | 0.460 | 0.434 | 12.5 |
| N ₂ | 450 | " ² | 0.330 | 0.258 | 0.118 | 0.419 | 0.267 | 0.387 | 29.0 |
| H ₂ | 350 | " | 0.219 | 0.197 | 0.287 | 0.665 | 0.470 | 0.438 | 17.3 |
| H ₂ | 450 | " | 0.290 | 0.168 | 0.199 | 0.464 | 0.334 | 0.323 | 28.8 |
| N ₂ | 350 | CdCl ₂ | 0.209 | 0.290 | 0.383 | 0.744 | 0.610 | 0.469 | 3.4 |
| N ₂ | 450 | " ² | 0.236 | 0.323 | 0.312 | 0.595 | 0.581 | 0.529 | 19.4 |
| H ₂ | 350 | " | 0.171 | 0.332 | 0.518 | 0.676 | 0.582 | 0.401 | 13.4 |
| H ₂ | 450 | " | 0.246 | 0.242 | 0.372 | 0.750 | 0.632 | 0.464 | 34.7 |
| N ₂ | 350 | CoCl ₂ | 0.280 | 0.407 | 0.539 | 0.858 | 0.708 | 0.536 | 2.4 |
| N ₂ | 450 | " ² | 0.240 | 0.231 | 0.335 | 0.773 | 0.592 | 0.488 | 17.5 |
| H ₂ | 350 | " | 0.244 | 0.396 | 0.525 | 0.888 | 0.703 | 0.591 | 2.4 |
| H ₂ | 450 | " | 0.269 | 0.324 | 0.415 | 0.735 | 0.630 | 0.571 | 26.7 |
| N ₂ | 350 | FeSO ₄ | 0.228 | 0.338 | 0.443 | 0.693 | 0.536 | 0.488 | 0.0 |
| N ₂ | 450 | " | 0.189 | 0.283 | 0.462 | 0.653 | 0.447 | 0.404 | 12.1 |
| H ₂ | 350 | " | 0.238 | 0.331 | 0.497 | 0.657 | 0.512 | 0.449 | 0.0 |
| H ₂ | 450 | " | 0.258 | 0.315 | 0.318 | 0.664 | 0.512 | 0.449 | 23.9 |

TABLE V
Multilinear Regression Analysis Correlation Coefficients

| Correlation | Coefficient | Correlation | Coefficient |
|-------------|-------------|-------------|-------------|
| 3030-2920 | -0.225 | 2850-1260 | +0.478 |
| 3030-2850 | -0.098 | 1610-1450 | +0.841 |
| 3030-1610 | -0.167 | 1610-1260 | +0.709 |
| 3030-1450 | -0.120 | 1450-1260 | +0.779 |
| 3030-1260 | -0.129 | 3030-V.M. | +0.289 |
| 2920-2850 | +0.785 | 2920-V.M. | -0.594 |
| 2920-1610 | +0.327 | 2850-V.M. | -0.557 |
| 2920-1450 | +0.234 | 1650-V.M. | -0.322 |
| 2920-1260 | +0.182 | 1450-V.M. | -0.119 |
| 2850-1610 | +0.353 | 1260-V.M. | -0.190 |
| 2850-1450 | +0.371 | | |

TABLE VI
Statistical Significance of I.R. Absorbance Data

ATMOSPHERE

| N ₂ or H ₂ | 3030 | | 2850 | | 3030/2920 | | 1610 | | % V.M. | |
|----------------------------------|------|-----|------|-----|-----------|-----|------|-----|--------|------------------|
| | S | E | S | E | S | E | S | E | S | E |
| ZnCl ₂ | --- | --- | --- | --- | --- | --- | --- | --- | 0.01 | I Hi T D Lo T |
| SnCl ₂ | --- | --- | --- | --- | --- | --- | --- | --- | --- | --- |
| CdCl ₂ | --- | --- | --- | --- | --- | --- | --- | --- | 0.05 | I |
| CoCl ₂ | --- | --- | --- | --- | 0.20 | D | --- | --- | --- | --- |
| FeSO ₄ | 0.05 | I | 0.05 | I | --- | --- | --- | --- | --- | --- |

TEMPERATURE

350 or 450°C

| | | | | | | | | | | |
|-------------------|------|-----|------|-----|------|-----|-------|-----|-------|---|
| ZnCl ₂ | --- | --- | --- | --- | 0.05 | I | 0.05 | D | 0.001 | I |
| SnCl ₂ | 0.01 | I | --- | --- | --- | --- | 0.001 | D | 0.001 | I |
| CdCl ₂ | 0.05 | I | --- | --- | 0.01 | I | --- | --- | 0.01 | I |
| CoCl ₂ | --- | --- | --- | --- | 0.01 | I | 0.05 | D | 0.001 | I |
| FeSO ₄ | --- | --- | 0.05 | D | --- | --- | 0.05 | D | 0.01 | I |

CATALYST EFFECT

| | | | | | | | | | | |
|-------------------|------|-----|------|-----|------|-----|-------|-----|------|-----|
| ZnCl ₂ | 0.05 | D | 0.20 | I | 0.01 | D | --- | --- | --- | --- |
| SnCl ₂ | 0.05 | I | --- | --- | 0.20 | I | 0.001 | D | 0.05 | I |
| CdCl ₂ | --- | --- | --- | --- | 0.05 | D | 0.05 | D | --- | --- |
| CoCl ₂ | --- | --- | --- | --- | 0.01 | D | --- | --- | --- | --- |
| FeSO ₄ | --- | --- | 0.01 | I | --- | --- | 0.01 | D | 0.20 | D |

S = Significance

E = Effect

I = Increase in measured absorbance

D = Decrease in measured absorbance

REFERENCES

1. R. A. Friedel, H. L. Retcofsky and J. A. Queiser, Advances in Coal Spectrometry-Absorbance Spectrometry, U.S. Bu. Min. Bul. 640, 1967.
2. R. A. Friedel and G. L. Carlson, "Difficult Carbonaceous Materials and Their Infrared and Raman Spectra, Reassignments for Coal Spectra," Fuel, 51, 194, (1972).
3. J. H. Shih, Y. Osawa and S. Fujii, "Infrared Spectra of Heat Treated Coal," Fuel, 51, 153, (1972).
4. H. H. Oelert, "Chemical Characteristics of the Thermal Decomposition of Bituminous Coals," Fuel, 47, 433 (1968).
5. J. K. Brown, "The Infrared Spectra of Coals" J. Chem. Soc., 744, 1955.
6. J. K. Brown, "Infrared Studies of Carbonized Coals," J. Chem. Soc., 752, 1955.
7. S. Fujii, Y. Osawa and H. Sugimura, "Infrared Spectra of Japanese Coal: The Absorption Bands at 3030, 2920 and 1600 cm^{-1} " Fuel, 48, 161, (1969).
8. W. H. Wiser, "A Kinetic Comparison of Coal Pyrolysis and Coal Dissolution," Fuel, 47, 475, (1968).
9. W. H. Wiser, L. L. Anderson, S. A. Qader and G. R. Hill, "Kinetic Relationship of Coal Hydrogenation, Pyrolysis and Dissolution," J. Appl. Chem., 21, 82 (March 1971).
10. B. K. Mazumdar, S. K. Chakrabartty and A. Lahiri, "Dehydrogenation of Coal and Tar Formation," Fuel, 38, 112 (1959).
11. B. K. Mazumdar, S. K. Chakrabartty and A. Lahiri, "Further Studies on the Dehydrogenation of Coals by Sulfur," Fuel, 41, 121 (1962).

CHARGE TRANSFER COMPLEXES OF COAL-DERIVED ASPHALTENES

I. Schwager, J.T. Kwan, J.G. Miller and T.F. Yen

University of Southern California
Chemical Engineering Department
University Park
Los Angeles, California 90007

INTRODUCTION

Coal-derived asphaltene are thought to be key intermediates in the conversion of coal to oil (1). A model, based on x-ray diffraction studies (2), has been proposed to describe the macrostructure of associated asphaltene in the solid state (3). The state of association of these species in benzene and tetrahydrofuran solution has been studied by vapor pressure osmometry, and molecular weights have been reported as a function of concentration (4). Evidence has been presented recently in the literature supporting a hydrogen-bonding donor-acceptor association in solution (5-7). Previously the mechanism of association of petroleum asphaltene (8-10), and coal and chars (11) was described in terms of charge transfer donor-acceptor forces. A study of the properties of iodine-petroleum asphaltene complexes was carried out, and led to useful information on the structure of petroleum asphaltene (12). It was therefore decided to synthesize charge transfer complexes of coal-derived asphaltene, and to study their properties by a variety of physical and analytical techniques.

EXPERIMENTAL

Coal-derived asphaltene were separated by solvent fractionation (13, 14) from coal liquids produced in five major demonstration liquefaction processes: Synthoil, HRI H-Coal, FMC-COED, Catalytic Inc. SRC, and PAMCO SRC. The asphaltene were further separated into three fractions by exhaustive solvent elution chromatography on silica gel using the solvents: benzene, diethyl ether, and tetrahydrofuran. The benzene and diethyl ether eluted fractions, known to contain a higher and lower proportion of basic asphaltene molecules (13), were used in addition to starting asphaltene to form some of the complexes.

Complexes were formed by mixing benzene solutions of the asphaltene (-50 g/l) with benzene solutions of either iodine or tetracyanoethylene (freshly sublimed reagent grade) in the approximate mole ratios, asphaltene/acceptor = 0.7 - 1.0/1. A precipitate forms rapidly. It was filtered, washed with benzene and dried overnight at 40°C/2mm Hg.

The dark brown to black I₂-asphaltene complexes are relatively insoluble in benzene, carbon disulfide, and pentane, and slightly to moderately soluble in chloroform and tetrahydrofuran. The brown-black TCNE-asphaltene complexes are only moderately soluble in THF.

Analyses were performed by the ELEK Microanalytical Laboratories, Torrance, California. Iodine was determined gravimetrically after nitric acid oxidation in the presence of silver nitrate; nitrogen was determined by the Dumas procedure. Molecular weights were measured in THF with a Mechrolab Model 301A Vapor Pressure Osmometer. Infrared spectra were determined as KBr disks on a Beckman Acculab 6 IR. Ultraviolet-visible spectra were run in either chloroform or tetra-

hydrofuran solution on a Beckman Model 25 Spectrophotometer. X-ray diffraction measurements were made with a General Electric XRD-6 x-ray diffractometer with a $\text{CuK}\alpha$ radiation source (15). Electron spin resonance spectra were taken with a Varian E-12 x-band spectrometer. Resistivity measurements were carried out at 25°C over the pressure range 10-3000 atmospheres by use of a cell and procedure described by Hadek (16).

RESULTS AND DISCUSSION

Composition of Complexes

Analytical data for I_2 -asphaltene and TCNE-asphaltene complexes are presented in Tables I and II. The mole ratios of asphaltene to iodine are approximately 1 to 1 with the exception of the FMC-COED - I_2 complex which afforded a tar-like material initially instead of a precipitate. The mole ratios of asphaltene to TCNE are more widespread, but are closer to 2 to 1. The mole ratio calculations are based on the assumption that the molecular weight of the asphaltene portion of the complex is the same as the molecular weight of the starting asphaltene, which may not be strictly correct.

Ultraviolet-Visible Spectra of Complexes

Measurement of the UV-Visible spectrum of I_2 -asphaltene complexes in THF or CHCl_3 (Fig. 1) leads to the observation of a new band at ≈ 295 nm and new shoulder at ≈ 355 nm. Neither of these absorptions is observed in the free components. These bands are presumed to be charge-transfer absorption bands of the iodine-asphaltene complex. The nature of the donor interaction of the asphaltene may be either via the electrons of the π -orbitals, or via the non-bonded, lone pair electrons in atomic orbitals of n donors such as nitrogen or oxygen bases.

Measurement of the UV-Visible spectrum of TCNE-asphaltene complexes in THF (Fig. 2) leads to the observation of new bands at 406 and 425 nm not found in the free components. These bands are presumed to be charge-transfer absorption bands of the donor asphaltene molecules and the π -acceptor TCNE.

Infrared Spectra

Asphaltene-iodine samples were run as KBr disks, and infrared spectra were obtained directly, and differentially of asphaltene-iodine complexes versus reference asphaltene. No C-I stretching frequencies were observed in the 400-600 cm^{-1} region, and no aromatic- I_2 bands in the 992 cm^{-1} to 1200 cm^{-1} region (17, 18).

Asphaltene-TCNE complexes were run in KBr disks and the infrared spectra compared with those of the free components, and physical mixtures of the free components. The most obvious changes are in the TCNE doublet at 2200 cm^{-1} which changes to a singlet, and in the appearance of a prominent new band at 1500 cm^{-1} .

X-Ray Diffraction

The x-ray diffraction patterns of asphaltenes show diffuse bands typical of mesomorphic or semicrystalline substances (2): the (002) band is attributed to the interplanar spacing between condensed aromatic rings of ≈ 3.5 Å; the gamma band is attributed to the spacing between disordered aliphatic chains or alicyclic rings of ≈ 4.6 Å (Fig. 3).

X-ray analysis of petroleum asphaltene-iodine complexes indicates a low degree of order exists within these complexes (12). The (002) band disappears on forming a petroleum asphaltene-iodine complex, and a new band at 8.7 Å appears. These observations were rationalized by assuming that the layered structure of the asphaltene was expanded from 3.5 Å to 8.7 Å by intercalation of a molecule of iodine between the aromatic layers of the asphaltene.

In the case of coal-derived asphaltene-iodine complexes, the x-ray results show the loss of both the (002) and the (γ) bands, but no new peak is formed at ≈ 8.7 Å (Fig. 3). This result may be interpreted by assuming that iodine molecules are not sandwiched between the aromatic layers, and that the asphaltene-iodine complexes are no longer ordered in the solid state but have become amorphous.

The x-ray diffraction patterns of asphaltene-TCNE complexes have been measured. The diffraction patterns show a large increase in the intensity of the 002-Band of the TCNE complex, which is associated with the interplanar spacing between condensed aromatic rings, and the appearance of a new band for Synthoil-TCNE, which corresponds to a larger distance of ≈ 11 to 14 Å. The x-ray diffraction patterns were analyzed, and aromaticity and x-ray crystallite parameters determined (Table III). The results indicate structural differences between the asphaltene base fractions (Et₂O eluted from silica gel) and their TCNE complexes. The aromaticity, f_a , increases from asphaltene base fractions to complexed products. The distance through the aromatic sheets, L_a , and the number of layers per cluster M are increased after complexing. However, the diameter of the aromatic sheet, L_a , shows a decrease or no change. The spacing between aliphatic chains or sheets, d_y , and the spacing between the aromatic sheets, d_m , do not show much change. These results, and the appearance of the new bands at 11-14 Å, may be rationalized in terms of asphaltene-TCNE complex clusters such as the ones shown in Fig. 4. If the TCNE molecules are complexed on top and below the asphaltene sheets, instead of intercalated between the asphaltene sheets, then an increase of L_c would be observed, but an increase in d_m or d_y would not be required. L_c , the average diameter of the aromatic sheet would be expected to be lower if a smaller TCNE molecule in the complex represented a pseudo-aromatic sheet. M , the effective number of aromatic sheets would be expected to be larger. The new bands corresponding to an 11-14 Å separation in Synthoil-TCNE could represent the distance between TCNE molecules in the complexes. The aromaticity, f_a , would be expected to increase in the complexes due to the pseudo-aromatic character of the TCNE π -system.

ESR Spectra

ESR parameters of Synthoil asphaltenes and their I₂ and TCNE complexes are presented in Table IV. The spin intensity is seen to be significantly larger in the complexes than in the uncomplexed asphaltenes. This may be indicative of low lying triplet states in the complexes which can be populated at room temperature.

Conductivity

The resistivities of a series of asphaltenes and their I₂ and TCNE complexes have been measured, and range between about 3×10^9 - 3×10^{10} ohm-cm at 25°C and 10 atm. pressure. In each case the resistivity of the complex is lower than that of the parent asphaltene, but not by more than an order of magnitude. These resistivities may be contrasted with those obtained for petroleum asphaltenes which exhibit higher values, in the insulator range, of 10^{16} - 10^{17} ohm-cm at 25°C, but upon addition of iodine, the resistivities of the complexes formed decrease by about one million-fold (12).

The effect of pressure, over the range 10-3000 ATM., on resistivity is shown in Fig. 5. The resistivity of the uncomplexed asphaltenes is seen to remain essentially constant, however, two of the asphaltene-I₂ complexes afford a decrease in resistivity over the same pressure range. This is consistent with electronic conduction.

ACKNOWLEDGMENT

This work was sponsored by the U.S. Department of Energy under contract no. E(49-18) 2031.

LITERATURE CITED

1. S. Weller, M.G. Pelpetz, S. Friedman, *Ind. Eng. Chem.* **43**, 1572 (1951); *ibid.*, p. 1575.
2. T.F. Yen, J.G. Erdman, and S.S. Pollack, *Anal. Chem.*, **33**, 1578 (1961).
3. T.F. Yen, Workshop on Coal Chemistry Preprint, Stanford Research Institute, 1976, pp. 144-164.
4. I. Schwager, W.C. Lee, and T.F. Yen, *Anal. Chem.*, **49**, in press, Nov. 1977.
5. H.N. Sternberg, R. Raymond and F.K. Schweighardt, *Science*, **188**, 49 (1975).
6. F.K. Scheighardt, R.A. Friedel, and H.L. Retcofsky, *Applied Spectroscopy*, **30**, 291 (1976).
7. S.R. Taylor, L.G. Galyla, B.J. Brown, and N.C. Li, *Spectroscopy Letters*, **9**, 733 (1976).
8. T.F. Yen, *Fuel*, **52** 93 (1973).
9. T.F. Yen and D.K. Young, *Carbon*, **11**, 33 (1973).
10. R.M. Elofson, K.F. Schulz, and B. Hitchon, *Geochimica et Cosmochimica Acta*, **41**, 567 (1977).
11. R.M. Elofson and K.F. Schulz, *Am. Chem. Soc., Div. Fuel Chem., Preprints*, **11**(2), 513 (1967).
12. G.A. Sill and T.F. Yen, *Fuel*, **48**, 61 (1969).
13. I. Schwager and T.F. Yen, *Am. Chem. Soc., Div. Fuel Chem., Preprints*, **21** (5), 199 (1976).
14. I. Schwager and T.F. Yen, Liquid Fuels from Coal, (R.T. Ellington, ed.), Academic Press, New York, 1977, pp. 233-248.
15. J.T. Kwan and T.F. Yen, *Am. Chem. Soc., Div. Fuel Chem., Preprints*, **21**(7), 67 (1976).
16. V. Hadek, *Rev. Sci. Instr.*, **42**, 393 (1971).
17. W. Haller, G. Jura, and G.C. Pimetel, *J. Chem. Phys.*, **22**, 720 (1954).
18. E.E. Ferguson, *Spectrochim. Acta*, **10**, 123 (1957).

Table I. Analytical Data for I₂-Asphaltene Complexes

| Asphaltene | VPO ^a MW | % Iodine | Asphaltene ^b /I ₂ |
|---|---------------------|----------|---|
| Synthoil | 560 | 35.02 | 0.84 |
| HRI H-Coal | 492 | 28.13 | 1.33 |
| FMC-COED ^c | 375 | 22.00 | 2.38 |
| PAMCO SRC ^d | 363 | 38.36 | 1.12 |
| CAT. INC. SRC | 483 | 32.72 | 1.08 |
| CAT. INC. Benzene Eluted 511 | | 30.34 | 1.15 |
| CAT. INC. Et ₂ O Eluted ^e | 459 | 34.03 | 1.08 |

^aAverage of infinite dilution MW's in benzene and tetrahydrofuran of starting asphaltene. ^bMole ratios calculated assuming MW of asphaltene portion of complex is the same as the MW of the starting asphaltene. ^cA tar formed on mixing the asphaltene/I₂ solutions. ^dFrom Filter Feed. ^eEluted from Silica Gel.

Table II. Analytical Data for TCNE-Asphaltene Complexes

| Asphaltene ^a | VPO ^b MW | ZN Complex - ZN Starting Asphaltene | Asphaltene ^c /TCNE |
|-------------------------|---------------------|-------------------------------------|-------------------------------|
| Synthoil | 522 | 5.08 ^d , 5.21 | 1.87, 1.82 |
| HRI H-Coal | 496 | 5.13 | 1.95 |
| FMC-COED | 383 | 5.48 | 2.34 |
| PAMCO SRC | 532 | 3.76 | 2.56 |
| CAT. INC. SRC | 459 | 7.61 | 1.33 |

^aAsphaltene eluted from Silica Gel with Et₂O after exhaustive elution of asphaltene with benzene. ^bAverage of infinite dilution MW's in benzene and tetrahydrofuran of starting asphaltene. ^cMole ratios calculated assuming MW of asphaltene portion of complex is the same as the MW of the starting asphaltene. ^dTwo different preparations.

Table III. X-Ray Analysis of Synthoil Asphaltene Basic Fraction and Synthoil Asphaltene-TCNE Complex

| | Synthoil Asphaltene Et ₂ O Eluted | Synthoil Asphaltene Et ₂ O Eluted-TCNE Complex |
|---------------------------------------|--|---|
| f _a ¹ | 0.64 | 0.72 |
| d _a ² | 3.47 | 3.46 |
| d _y ² | 4.52 | 4.52 |
| l _c ² | 12.1 | 13.8 |
| L _a ³ (11) band | 10.0 | 10.1 |
| L _a ⁴ (11) band | 11.4 | 11.9 |
| M ⁵ | 4 | 5 |

¹f_a = C_A/C_{total} = A₀₀₂/A₀₀₂ + A_y, ²d_a = interlayer distance, d_y = interchain distance, l_c = diameter of the aromatic clusters perpendicular to the plane of the sheets, L_a³ = diameter of the aromatic sheets from Diamond's Curve, L_a⁴ = diameter of the aromatic sheets from Scherrer's Eq., all values in Å. ⁵Effective number of aromatic sheets associated in a stacked cluster.

Table IV. ESR Parameters of Asphaltenes and Asphaltene Complexes^a

| Sample | g-Value ^b | Intensity, N (x10 ¹⁸) Spins/g | Line Width ΔH, Gauss |
|--|----------------------|---|----------------------|
| Synthoil Asphaltene | 2.0030 | 1.4 | 6.4 |
| Synthoil Asph. Et ₂ O Eluted | 2.0031 | 0.8 | 6.8 |
| Synthoil Asph.-I ₂ Complex | 2.0032 | 28.8 | 9.8 |
| Synthoil Asph. Et ₂ O Eluted-TCNE Complex | 2.0029 | 5.5 | 8.2 |

^aSolid samples. ^bMeasured relative to DPPH.

FIG. 1. UV-VIS. SPECTRA OF I_2 , SYNTHOIL ASPHALTENE, AND SYNTHOIL ASPHALTENE- I_2 COMPLEX IN $CHCl_3$

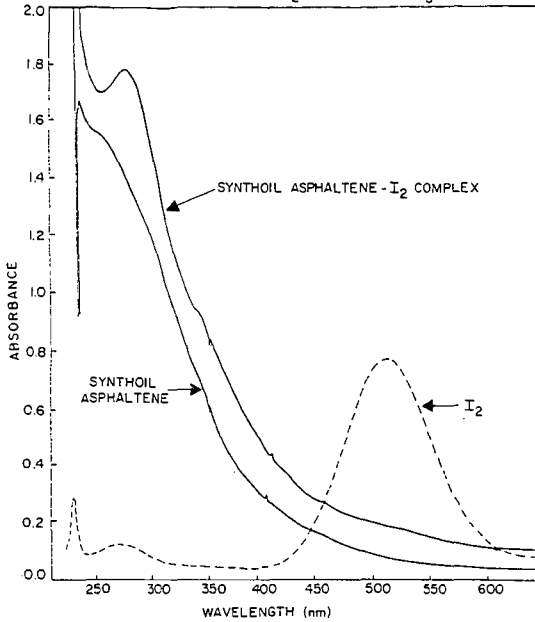


FIG. 2. UV-VIS. SPECTRA OF TGNE, SYNTHOIL ASPHALTENE, AND SYNTHOIL ASPHALTENE-TGNE COMPLEX IN THF

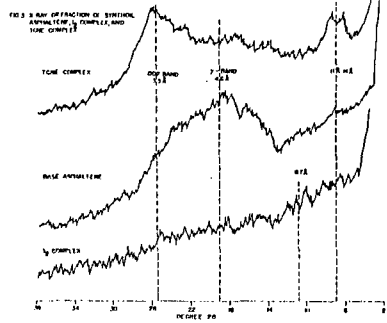
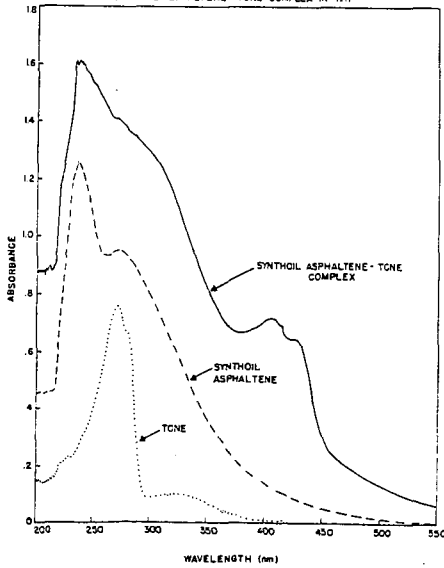


FIG. 4. CROSS-SECTIONAL VIEW OF SYNTHOIL ASPHALTENE BASE FRACTION AND SYNTHOIL ASPHALTENE-TGNE MODEL COMPLEX CLUSTERS

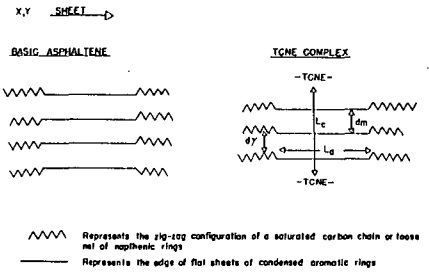


FIG. 5. RESISTIVITY OF CAT. INC. SRC. ASPHALTENE, ASPHALTENE DERIVATIVES, ASPHALTENE COMPLEXES VS. PRESSURE

